Universitatea Transilvania din Brașov

INTERDISCIPLINARY DOCTORAL SCHOOL
Faculty of Product and Environmental Design

Drd. ing. Denisa Ioana RUSEA

Colectoare solar termice de forme diverse implementabile în mediul construit

Solar thermal collectors of different shapes implemented in the built environment

SUMMARY

Scientific leader
Prof. em.dr. ing. DHC Ion VIȘA

BRAȘOV, 2024

CONTENT

Introduction

In a top 10 list of the problems humanity will face by 2055, Nobel laureate Richard Smalley puts energy at the top of the list and points to the importance of energy in alleviating the other problems: water, food, environment, poverty, terrorism, wars and democracy (Smalley, 2005).

At regional and national level, actions and regulations have been generated to limit the negative effects of development on communities. As an example at the European level, there is the 2020 Directive (RED II Directive), on increasing energy efficiency, reducing the amount of GHGs (greenhouse gases) and increasing the deployment of renewable energies. Another regulation is the Energy Performance of Buildings Directive (2018/844, EU) which imposes standards and targets to increase the energy efficiency of buildings. The European Green Deal (Green Deal, 2019) proposes climate neutrality by 2050 and a transition to a green economy.

The current energy pattern based on fossil fuels has had a negative impact on mankind: the continued increase in greenhouse gases, global warming, climate change, environmental degradation and a severe depletion of raw material reserves for energy production and product development.

Global statistics show that today more than 80% of energy comes from fossil fuels (82%), with the highest percentage coming from oil (30.5%), followed by coal (26.9%) and natural gas (24.5%). About 18% of energy comes from renewable sources, more than half of which comes from hydro (6.8%), followed by solar and wind (4.6%).

Together with the main economic sectors (industry, transportation, agriculture), the built environment is responsible for approximately 30% of global energy consumption and 26% of GHG (Greenhouse Gas) emissions at European level. Energy is used in the built environment mainly for domestic hot water, space heating and cooling.

Among the sources of energy production in the built environment, solar energy has an accentuated dynamic through solar-thermal and solar-electric conversion and can replace fossil fuels.

By using a solar thermal collector it is possible to provide in Central and Eastern Europe useful thermal energy in the built environment (at 40...60°C) for the main residential applications: domestic hot water (DHW) preparation, preparation of thermal agent for heating and cooling of rooms respectively. The amount of thermal energy produced by a solar thermal collector provides almost all of the domestic hot water needs throughout the year, except for short periods of 1-2 months at the beginning and end of the year, when the DHW needs are partially covered. As for space heating, full coverage of the heating needs can be achieved for a maximum of 2 months (in April and October), a small part of the needs is provided for about 2 months (in March and November), and in the remaining cold months (January, February and December) the heating contribution is practically zero. As a result, solar-thermal conversion cannot be the basic source for space heating. In terms of thermal energy demand for cooling (during the period May-September), the thermal energy produced by the collector provides almost the entire thermal energy demand. A similar analysis can be made for other areas, where the location, size and conditions of implementation of solar thermal systems determine the degree of coverage of the three functionalities in the built environment.

Solar thermal systems are placed either on buildings in the built environment (roof, facades), or near buildings (on specially designed structures), or on buildings or near thermal

power plants intended to provide thermal energy for entire areas of individual or collective housing, or even in the form of solar thermal parks with energy storage in large boilers.

Increasing the amount of thermal energy through solar thermal conversion involves increasing the areas of solar thermal collector placed on buildings, while at the same time increasing the architectural accenptance in the energy efficient built environment. It involves the promotion of new types of solar thermal collectors of unconventional shapes and appropriate colors.

This thesis promotes, in this sense, solar thermal collectors of equilateral triangle and isosceles trapezoidal shapes, which by combinations it can define various collector structures of different sizes and colors, which ensure both an increase in the degree of coverage of the available surfaces in buildings and the aesthetics of their layout.

1. The current stage in the production of thermal energy in the built environment

In the context of rapid global population growth and accelerated urbanization, the built environment plays an important role in shaping a sustainable future. To face the challenges of climate change and depletion of natural resources, a sustainable approach to the design, construction and management of buildings and urban infrastructure is absolutely necessary to provide a sustainable future for next generations.

Depending on the type, purpose and activities carried out in the building, four main types of built environment can be distinguished:

- - *the residential built environment* for residential use, made up of individual houses, apartments, blocks of flats, which in turn form associations of buildings called districts or blocks;
- - *the commercial built environment* which refers to utilities available to citizens such as shops, leisure centers, hotels;
- - *the administrative built environment* which is made up of state institutions destinated for the utility, education or administrative management of the community;
- - *the industrial built environment*, to which production or storage establishments belong.

Taking into account that the residential sector occupies 75% of all buildings in the European Union, the major problem is the provision of thermal energy in the residential built environment. Non-residential buildings include: shopping centers (28%), offices (23%), educational institutions (17%), hotels or restaurants (11%), hospitals (7%), sports halls (4%) or other buildings with different public purposes (Bointner et.al. 2014).

By using different technologies both passively and actively, solar energy can be used to design a building in an energy efficient way. In the passive mode, the building design is done maximizing the use of solar radiation, e.g. facing south to benefit from daylight throughout the day and having integrated windows for natural daylighting; and in the active mode, technologies can be used in the built environment to capture solar radiation and convert it into electricity or heat (Table 1.1).

In context of efforts to reduce dependence on fossil fuels and to adress climate change, a central component of this is the transition to renewable energy sources, and solar energy is the most affordable, efficient and environmentally friendly solution.

Table 1.1.Characterization of active and passive means of building a sustainable environment

Ways to develop sustainable built environment	Implementation opportunities	Materials that can be used
PASIV	Building orientation	south facade
	Thermal insulation	basalt wool, mineral wool, extruded polystyrene
		thermopane windows
		shading shutters
	Natural ventilation	slits, vents
	Natural light	windows, dormer windows
ACTIV	Photovoltaic solar systems	solar photovoltaic panels
	Solar thermal systems	solar thermal collectors
	Advanced insulation and efficient heating/cooling systems	sensors to monitor temperature, humidity
		controllers to manage lighting or air conditioning systems
	Use of environmentally friendly materials	thermal insulation materials: glass wool insulation
		low carbon footprint concrete (geopolymer cement)
		recycled materials (glass, plastic)
		sustainable wood: bamboo

Depending on the passive or active alternatives used in the construction of a building, four main building types are distinguished according to the level of energy consumed::

a. _Traditional buildings with high energy consumption_ – are uninsulated buildings using non-renewable sources for energy consumption (≤ 250 kWh/m^2/an);

b. _Low Energy Building (LEB)_ – represent around 50-60% from all buildings, have significantly lower energy consumption than traditional buildings, high thermal efficiency and can use renewable energy systems (SER). There are three types:

i. _nZEB (Nearly zero energy building)_ - are buildings with low energy consumption from conventional sources;

ii. _ZEB (zero energy building)_ – buildings without energy consumption from conventional sources;

iii. _PEB (Plus Energy building)_ – active buildings that produce more energy from renewable sources than they consume.

c. _Passive houses_ – energy efficient buildings, designed to reduce energy needs through passive methods such as the use of thermal insulation, south-facing to use as much natural light as possible. They consume up to 90% less thermal energy than conventional buildings, have low emissions and can actively or passively use renewable energy.

d. _Greed building_ – green buildings made from environmentally friendly raw materials (e.g. wood, timber, timber) with very low waste and emissions. (Vişa et.al., 2020)

In Romania, the majority of buildings have high thermal energy consumption, as they are traditional houses.

Providing thermal energy in the built environment can be achieved from both from fossil fuels and from natural sources (Fig.1.1):

a. Traditional sources: natural gas, oil, coal, nuclear;
b. Renewable sources: solar, geothermal, biomass, wind, hydro, etc.
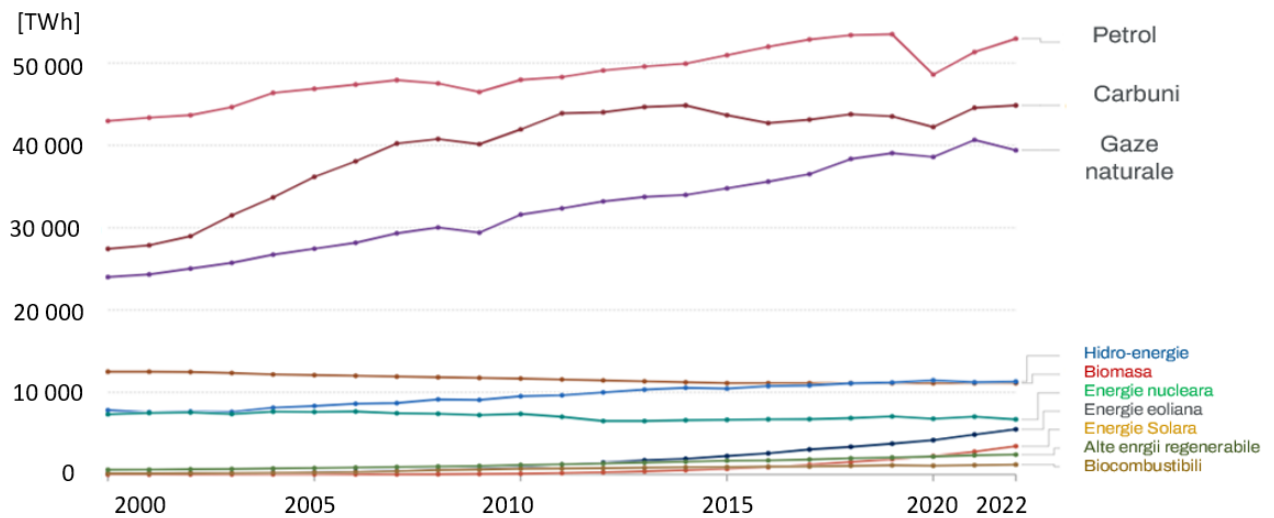**c. Traditional combined with renewable sources**

Fig. 1.1 Changes in the amount of energy consumed globally from all resources
(IEA processed - Satistic Review 2023)

The benefits of using clean sources are significant: reducing the carbon footprint, conserving limited resources, minimizing emissions and environmental pollution. Promoting energy efficiency or increasing the resilience and sustainability of communities are just some of the positive aspects of using these sustainable solutions.

Renewable energy systems are increasingly being used in the community due to their benefits over fossil fuels. They are mainly used for the production of thermal energy, and convert solar energy using the main element: solar thermal collectors.

Different types of solar thermal systems are available according to the thermal agent used, the geographical location and the climate of the area in which it is implemented:

- **Natural circulation/thermosiphonage systems** – have few components and low costs. They cannot operate at negative temperatures, and the storage tank must be positioned at the top of the collector, needing a positioning structure and leaving an unpleasant appearance (Fig.1.2.a).

- **Forced circulation systems** – open/closed circuit - components: boiler, auxiliary source, pumping group (P), expansion vessel (VE), controller, flow meter (D) and temperature sensors (T). Can operate at negative temperatures and can be integrated into the building envelope (Fig.1.2.b).
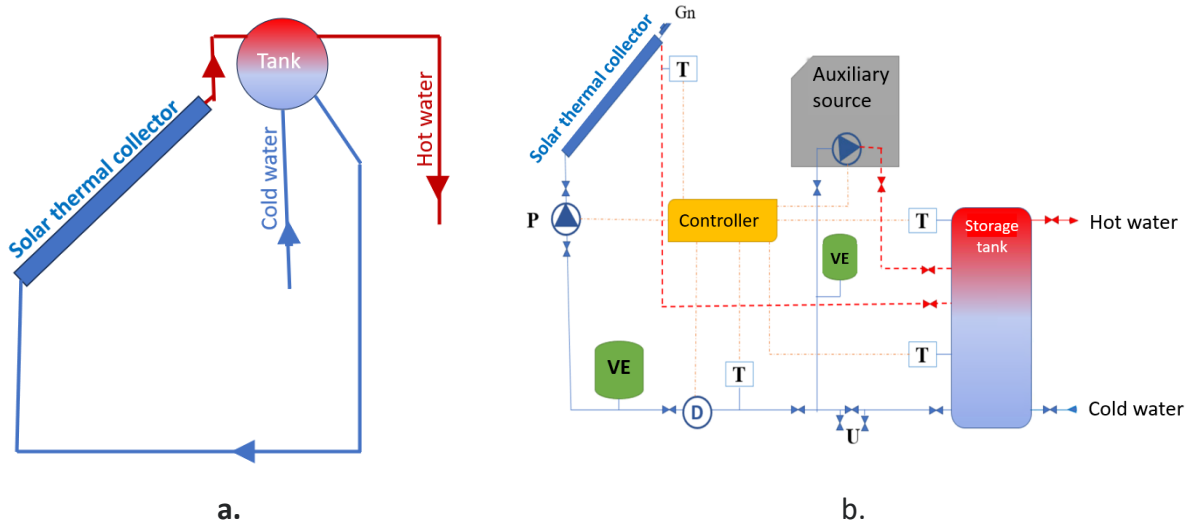

a.   b.

Fig.1.2. Schematic representation of a solar thermal system: a. With natural circulation; b. With forced circulation and auxiliary source.

Solar thermal collectors (STCs) are the main component of a solar-thermal system, converting solar radiation into thermal energy.

The principle of operation is based on heat transfer from the absorber plate (1) to the thermal agent. The heat is then transported through the pipes of the solar thermal system (3) to a storage tank where it is stored for use in space heating or domestic hot water preparation (Fig. 1.3).

The STC can be classified according to working temperature into:

- low temperature solar thermal collectors used for water heating (e.g. for swimming pools);

- medium temperature solar thermal collectors (for space heating or domestic hot water);

- high temperatures solar thermal collectors (solar concentrators used for electricity generation) (Bhatia, 2014).

The main components of a thermal solar collector are shown in the figure 1.3:

1. **Glazed surface;**
2. **Absorber plate;**
3. **Copper serpentine;**
4. **Posterior and lateral thermal insulation;**
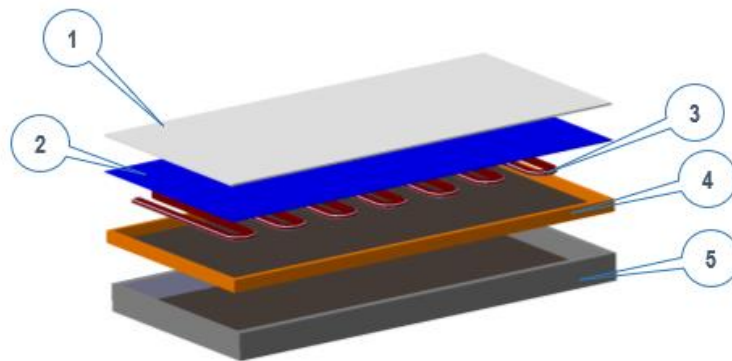5. **Metal case.**

6.

Fig.1.3. Components of a flat plate solar thermal collector: 1- glazed surface; 2-absorber plate; 3-serpentine; 4- thermal insulation; 5- metal case.

CST can be placed wher the metal support allows it to be fixed: on roofs, on facades, next to buildings, as shading elements on terraces or integrated into balconies or windows. There are also STCs of different shapes but with low efficiency for water heating used for swimming pools: spherical, hemispherical, conical, tubular. Or STCs developed for integration into the roof of the building, such as solar tiles, or sandwich panels integrated into building facades.

The collectors proposed for implementation on building facades, developed in the RESREC Research Center of Transilvania University of Brasov, can be disposed not only as individual entities, but as interconnectable modules. Starting from the basic geometrical shapes, the concepts were developed starting from the equilateral triangle (Fig. 1.4.a); the developed triangular collector is composed of: glazed surface (1), absorber plate (2) with a cavity replacing the coil and the metal casing together with the thermal insulation (3) (Fig. 1.4.b). An isosceles trapezoid can be created from three such triangles side by side (Fig. 1.5.a). The two shapes triangle and trapezoid form the basis for the development of a new chapter on the evolution of flat-plate solar thermal collectors.
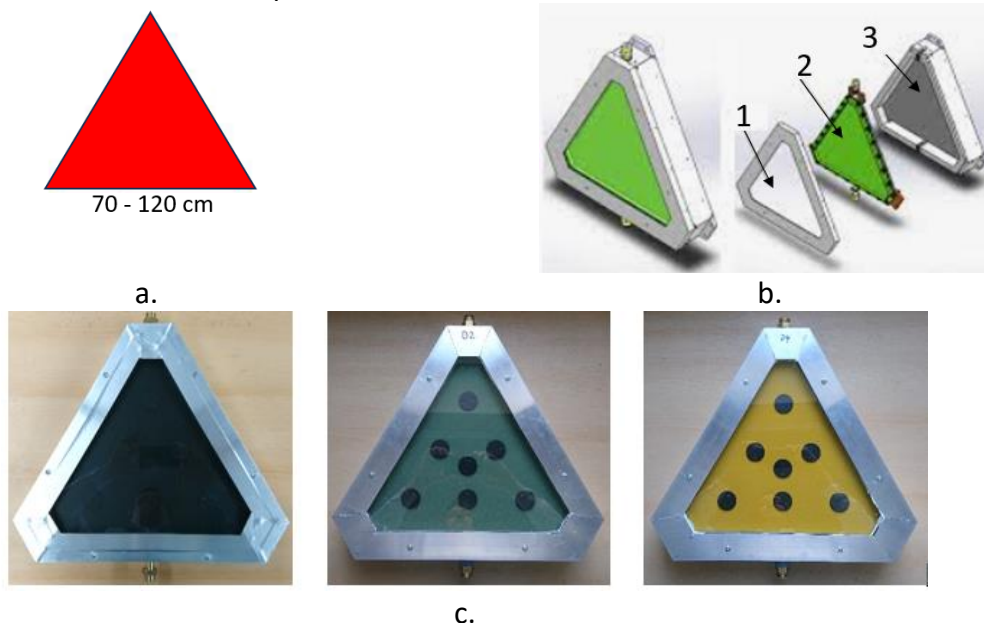

a.

b.

c.

Fig. 1.4. STC trunghiulare: a. The proposed concept (Vișa et.al., 2014);b. 3D model of the triangular STC (Moldovan et.al., 2020);
c. Physical version of 3 triangular STC from the research center RESREC

70 – 120 cm

70 – 120 cm

140 – 240 cm

Glass surface

New spectral-
selective absorbers

Trapeze
serpentine

Thermal
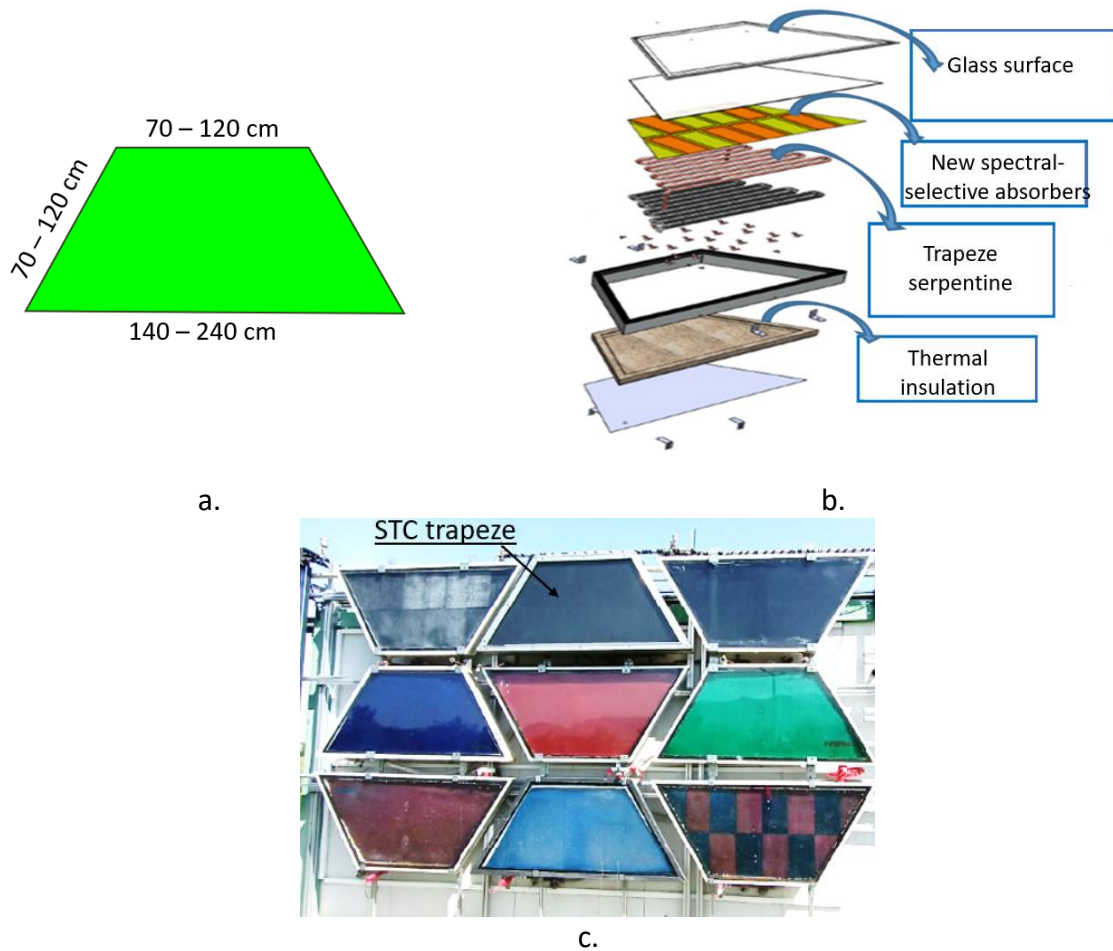insulation

a.

b.

STC trapeze

c.

Fig. 1.5. Trapezoidal collectors of different colors: a. Proposed concept (Vişa et.al., 2014); b. 3D model of the trapezoidal collector (Vişa, EST IN URBA Project, 2012); c. Physical version of 9 trapezoidal STC installed in the RESREC Research Center in Brasov

New equilateral triangle and isosceles trapezoidal CSTs open a new chapter in the deployment of renewable energy systems in the built environment. The lego assembly allows them to be placed in places that are difficult to reach for a classical STC (Fig. 1.6).

Thus, by using solar thermal collectors to provide the increased thermal energy demand, the built environment is facing new challenges in the field of solar thermal collector integration in terms of the need to increase the coverage of available surfaces and the degree of architectural acceptability. Based on this challenge, ways to develop new types and combinations of solar thermal collectors and their integration into the built environment were analyzed.

In this context, new shapes of trapezoidal and triangular STC are proposed that can be combined in the form of subassemblies, they can generate different design patterns inspired by nature, art models or old house architecture. By combining collectors of the same or different shapes, symbols, logos or 3D designs can be generated. By increase the color pattern for the absorber plate will be improved and harmonized the visual appearance. The connection with the rest of the building's construction elements is made through the color image.

Fig. 1.6. Comparison of commercial vs. trapezoidal collector solar facades
(Vișa et.al., 2017)

The aim of the research is to design and develop solar thermal collectors of unconventional shapes implementable in the built environment to increase solar fraction and architectural acceptability.

2. Thesis objectives

General research objective

Increase thermal energy and architectural acceptability by developing and using solar thermal collectors in unconventional shapes and different colors.

The operational research objectives are:

O1. Analysis of the current stage in the production of thermal energy in the built environment through solar thermal conversion.

O2. Design of solar thermal collector configurations consisting of unconventional equilateral triangle and isosceles trapezoid collectors with serpentine and possible applications.

O3. Study of the thermal efficiency of triangular solar thermal collectors with serpentine and identification of the optimal solar thermal collector.

O4. Design, development, execution and indoor/outdoor testing of the optimal triangular solar thermal collector with serpentine for proof of concept.

O5. Research conclusions and contributions.

2. The concept of solar thermal collector assemblies consisting of unconventional collectors

In general, solar thermal collectors are deployed on the roof of buildings or in the space around the house to produce thermal energy for domestic hot water or space heating. However, the acceptance of building envelope integrated solar systems has many limitations in terms of aesthetics (Schüler, 2003). The major problems of integrating ordinary solar thermal collectors into the building environment are the size, shape and the usual color of the absorber plate (shades of blue, black). The development of new solar thermal collectors offers the possibility to implement them in other places as well, i.e. creating solar thermal facades.

In the RESREC Research Center of Transilvania University of Brasov, new concepts of flat plate solar thermal collectors of various shapes (equilateral triangle and isosceles trapezoid) with different colors of the absorber plate (red, green, yellow, purple, black) have been developed. In particular, three types of structures has been developped containing: Fe_2O_3, V_2O_5 and CuS which helped to produce the absorbent tiles in the colors red, yellow and dark green (Vişa et.al., 2017).

The main characteristics that influence urban aesthetics are:
* *Size and position of solar thermal collectors;*
* *Shape and size of solar thermal collectors;*
* *Type of joint;*
* *Materials and their texture;*
* *Color of the absorber plate*.

2.1 Configurations obtained by combining STC of unconventional shapes

The design of subassemblies consisting of triangular and trapezoidal flat-plate solar thermal collectors should follow several rules to achieve architectural acceptance. In order to increase the quality of integration of solar thermal collectors into the built environment, the whole design can be created in such way that it is representative for different types of users. In this perspective, some important features will be considered:
* Different geometries/sub-assemblies, based on the following shapes: equilateral triangle and isosceles trapezoid, with all sides, except the large base, equal to the side of the triangle.
* Extend the color spectrum to achieve the 3D effect of the whole design.
* Various applications for:
  o Traditional facades;
  o Modern façades;
  o Flexible design (making logos or various artistic images).

In order to identify how the STCs are combined, it is necessary to code them and the links between them in subsequent applications; thus, reference will be made to the triangle with lowercase letters, and to the trapezoid with uppercase letters except for the lowercase base, according to Fig.2.2:

- Triangle: **t**;
- Trapeze: **T**;
- Side of triangle: **e** (edge);
- Small trapeze base: **b**;
- Large trapeze base: **B**;
- Non-parallel side of the trapezoid: **L**.

Based on them, new sub-assemblies were realized using <u>two elements</u>:
- 2 Triangles: **2t**;
- 2 Trapezes: **2T**;
- 1 Triangle and 1 trapeze: **1 tT**.

Respectively sub-assemblies of <u>three component</u>:
- 3 Triangles: **3t**;
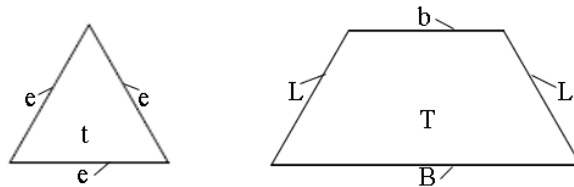- 3 Trapezes: **3T**;
- 2 Triangles and 1 trapezed: **2tT**;
- 1 Triangle and 2 trapezes: **t2T**.

Fig.2.1. Coding of triangular and trapezoidal solar thermal collectors

Starting from the two basic shapes, derived shapes can be represented by assembling 2 or 3 basic shapes according to different criteria.

a)   Subassemblies consisting of 2 units having common sides

In the case of the subset of two triangles with a common side, only one configuration is possible, shown in Fig.2.2:
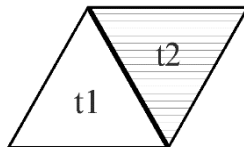
Fig. 2.3 The subassembly formed by two triangles with a common side, "*tt*"

In the case of the subassembly consisting of two trapezoids, the matrix in Fig. 2.3. is designed, resulting in 9 possible variants, 3 of which are doubled, highlighted in blue. Thus from two trapezoids 6 distinct subsets can be formed.

TT		Laturile T2		
		b	**B**	**L**
Laturile T1	**b**	bb	bB	bL
	B	Bb	BB	BL
	L	Lb	LB	LL

Fig.2.3. The concept matrix of the subassemblies formed by two trapezes

Based on the 6 possible concepts, in Fig. 2.4 the **12 possible design configurations** are made, of which similar pairs are found: **bB și Bb, bL și Lb, BL și LB**, so that the unique variants left in the matrix are in number of **6**. Due to the fact that the trapezoid has 2 non-parallel sides, it is possible to attach them to the second trapezoid in different ways, which is why in combinations containing one of the non-parallel sides, several design variants will be observed.
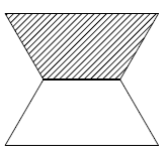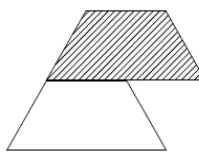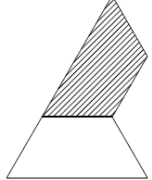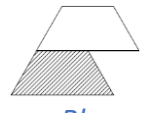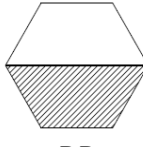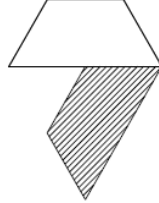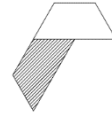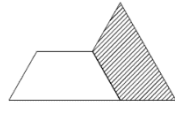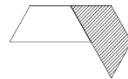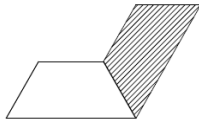

Fig.2.4. Subassemblies consisting of two traps with a common side, *TT*

Following the same algorithm, variants can be generated using a triangle and a trapeze (1t +1 T) in Figure 2.5. The construction mode keeps the trapeze as the base, to which the triangle is added one at a time on the sides of the trapezoid.

Fig. 2.5. Subassemblies *1t + 1 T*

b) Subassemblies consisting of 2 units having a common tip/vertex

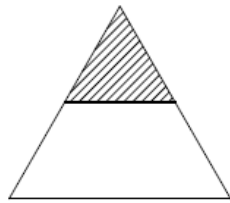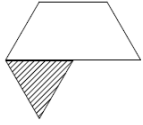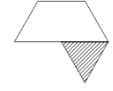Sub-assemblies of two units with a common tip can be realized, but they require a large supporting surface, and the fluid inlets and outlets from the solar thermal collectors may be difficult to realize, resulting in higher heat losses due to pipe joints outside the modules. Also, considering the hypothesis of mass production of such subassemblies, the necessary storage space, the metal structure needed to support the subassemblies as well as their packaging and transportation would be difficult to realize, requiring more space that remains unused. Therefore, it is more advantageous to add the units as individual parts, which can in turn be arranged according to the user's requirements.

For subassemblies consisting of two units with a common peak, a new index is introduced to code the resulting variants:

- Common tip, is called vertex „**v**" for triangle and „**V**" for trapeze, followed by the value of the angle between the 2 edges.

As an example, there are two possible ways of realizing a subset of two triangles with a common vertex in Fig. 2.6, 6 main variants and 3 secondary variants for subsets of two trapezoids, în Fig. 2.7.

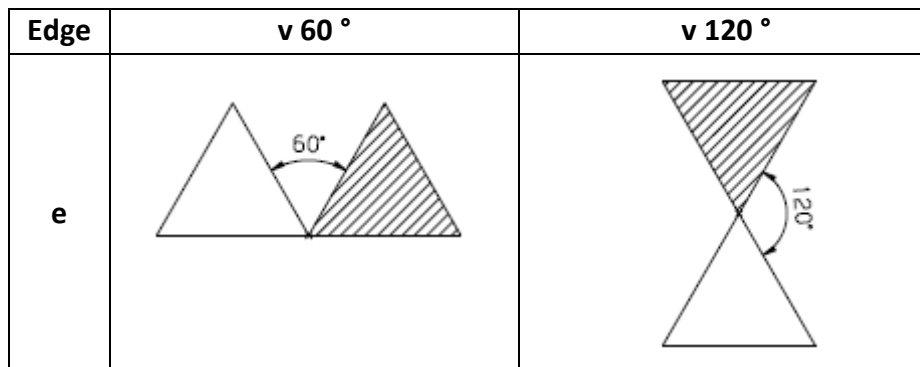| Edge	v 60 °	v 120 °
e		

Fig. 2.6. Subassemblies of two triangles with a common vertex

To simplify the way to join the two trapezoids with a third shape, the angle formed between the two shapes must be divisible by 6 (thus making it possible to join another triangle or trapezoid: 0°, 60°, 120°, 180°, 240°, 300° și 360°).

This keeps the reference trapezoid in the same position for each variant. It obtains 6 variants by rotate with 60° offset around the clock like in figure 2.7: no. 1 is the reference trapeze, on it are noted the two vertices where the second trapezoid can be connected: either at the 60° vertex between the large base and a non-parallel side, noted **VB**, either the 120° angle between the small base and the non-parallel side, noted **Vb** for simplification; so reference trapeze No. 1 can be positioned at 60° in variants No. 2 to No. 6.

In order to obtain variants of two trapezoids with a common vertex, some rules are imposed to determine a number of 6 principal variants:

- Reference trapeze T1 maintains its position (la 0°, 60°,120°, 180°, 240°, 300°).
- Trapeze T2 is maintained at position 1, at 0°.
- Variants of 2 trapezes are formed by attaching to the trapeze T2, which remains at 0°, the reference trapeze T1 by locating it at each of the vertices of T2 starting with the left/right vertices of the small base, then the left/right vertices of the large base.

Since the trapezeT2 is maintained at 0°, the resulting variants are easier to visualize and realize.

- The coding of variants follows the model

Vertez of trapeze T1 with index of trapeze position T1+ „−" + angle between T1 and T2 + „−" + Vertez of trapeze T2 with index of its position;

- Identify the variants where the attached trapeze T2 is in contact with each of the 4 vertices of the reference trapeze T1.

From figure 2.7 identifies the reference trapeze T1 represented by the hatched line.
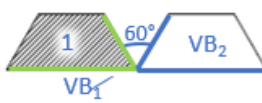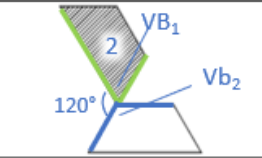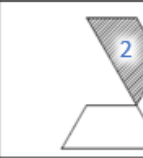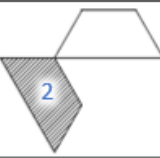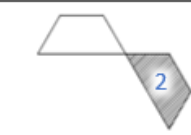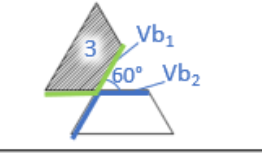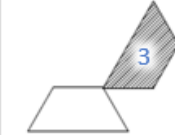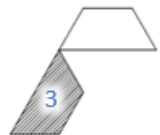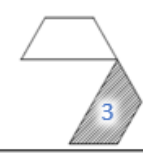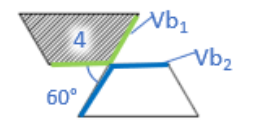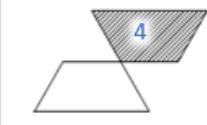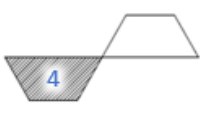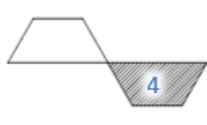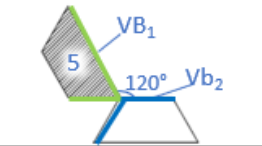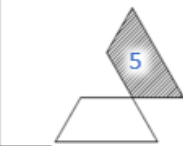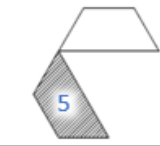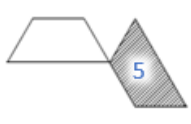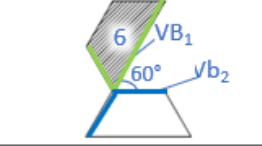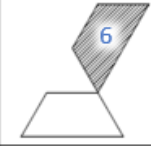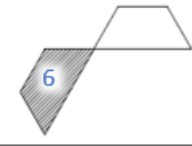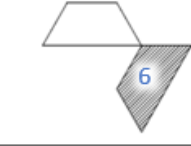
TT \ T1	Principal variant	Secondary variants		
0° / 1				
VB_0	$VB_0\text{-}60\text{-}VB_0$	$VB_0\text{-}60\text{-}VB_0$	$VB_0\text{-}60\text{-}Vb_0$	$VB_0\text{-}60\text{-}Vb_0$
60° / 2				
VB_{60}	$VB_{60}\text{-}120\text{-}Vb_0$	$VB_{60}\text{-}60\text{-}Vb_0$	$Vb_{60}\text{-}60\text{-}VB_0$	$VB_{60}\text{-}120\text{-}VB_0$
120° / 3				
VB_{120}	$Vb_{120}\text{-}60\text{-}Vb_0$	$VB_{120}\text{-}120\text{-}Vb_0$	$VB_{120}\text{-}60\text{-}VB_0$	$VB_{120}\text{-}60\text{-}VB_0$
180° / 4				
VB_{180}	$Vb_{180}\text{-}60\text{-}Vb_0$	$Vb_{180}\text{-}60\text{-}Vb_0$	$VB_{180}\text{-}120\text{-}VB_0$	$VB_{180}\text{-}120\text{-}VB_0$
240° / 5				
VB_{240}	$VB_{240}\text{-}120\text{-}Vb_0$	$Vb_{240}\text{-}60\text{-}Vb_0$	$VB_{240}\text{-}60\text{-}VB_0$	$Vb_{240}\text{-}120\text{-}VB_0$
300° / 6				
VB_{300}	$VB_{300}\text{-}60\text{-}Vb_0$	$VB_{300}\text{-}60\text{-}Vb_0$	$VB_{300}\text{-}120\text{-}VB_0$	$Vb_{300}\text{-}60\text{-}VB_0$

Fig.2.7. Subassemblies of two trapezes with a common vertex

c) Subassemblies consisting of 3 units having common sides

Starting from the distinct concepts of 2 geometric shapes, a third shape was added to generate new variants, taking into account only the variants with a common side exemplified above.

For subassembly **2t**, there is only one possibility to attach the third triangle to the already existing configuration, available in figure 2.8.

3t	ee
e	
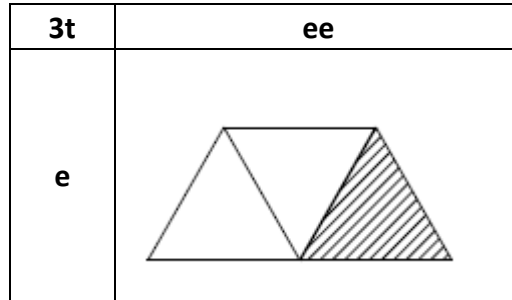
Fig. 2.8 Subassembly of three triangles, *3t*

Subassemblies of 3 trapeze are formed by attaching a trapeze to each of the variants resulting from the combination of two trapeze, considered as the reference shape.

Coding of the assembly is done according to the model:

Basic figure code (root) + „ -" + side of the base figure + attached side of the third trapeze.

Eg: **bb-Bb** corespond to: small base + large base (root **bb**) **–** the large base of the root to which the small base of the third trapeze is attached (**Bb**).

Rezults 48 variants:6-bb, 9-bB ,9-bL , 6-BB , 9-BL and 9-LL.

For example for the base „**bb**" the 6 possible options are presented in Fig. 2.9.
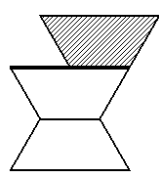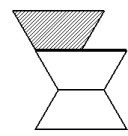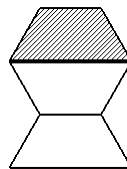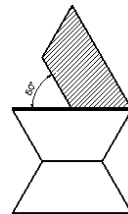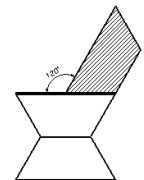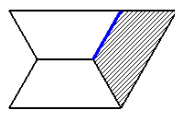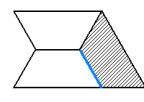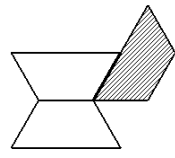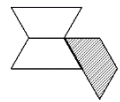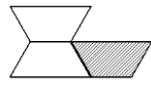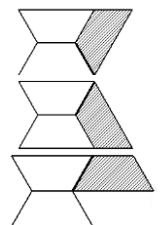
bb	b		B	L	
B	bb-Bb	*Variant*	bb-BB	bb-BL	*Variant*
L	bb-Lb	*Variant*	bb-LB	*Variant*	bb-LL	*Variant*

Fig.2.9. Possible subassemblies consisting of 3 trapezes, starting from the base „bb"

Subassemblies can also be formed from 3 distinct units: two triangles and a trapezoid or two trapezoids and a triangle. For variant „**2t"+ T** 3 models can be generated depending

on the position of the assembly „2t" on each of the sides of the trapezoid. For variant „2T"+ t" 19 models can be generated (2-bb , 3-bB ,3-bL , 2-BB , 3-BL , 3-LL) starting from „2T" shown previously and attaching the triangle to each of the sides of the trapeze.

The hydraulic interconnection of the subassemblies can be done as follows: for the triangle, the entry/exit of the thermal agent can be done through the top and the middle of the opposite side, and for the trapeze through the small base, respectively through the large base.

2.2 Increasing architectural acceptance by using different colors and pseudo 3D concept

Architectural acceptance can be achieved by integrating different colors into the built environment. In this way, solar thermal facades can be created from collectors of different colors to be used as decoration elements, not only for their ability to produce thermal energy. If the color palette for the absorbent plate of STC is developed, design elements can be created that surprise by using contrasting colors, which can apparently reproduce the 3D effect. For example, in Fig. 2.10 are groups of CSTs that use contrasting colors to form the images of boxes/cubes: the shadow effect is achieved by adding a darker color next to a lighter one, eg: yellow/orange vs. brown/green/black.

a)   b)
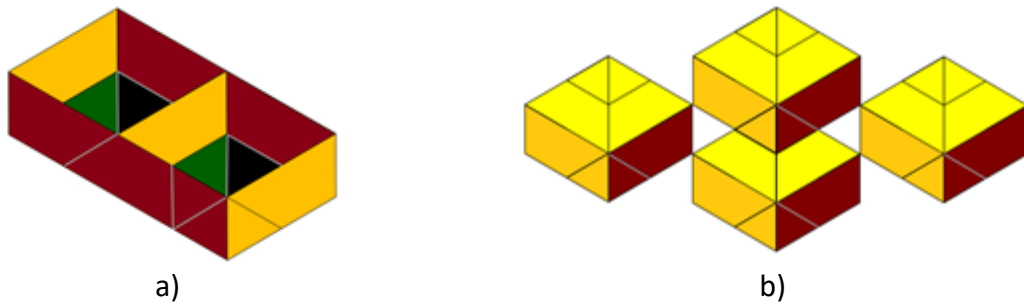
Fig. 2.10. Pseudo 3D design using triangular and trapeze STC subassemblies.

a)   b)   c)

d)   e)   f)   g)
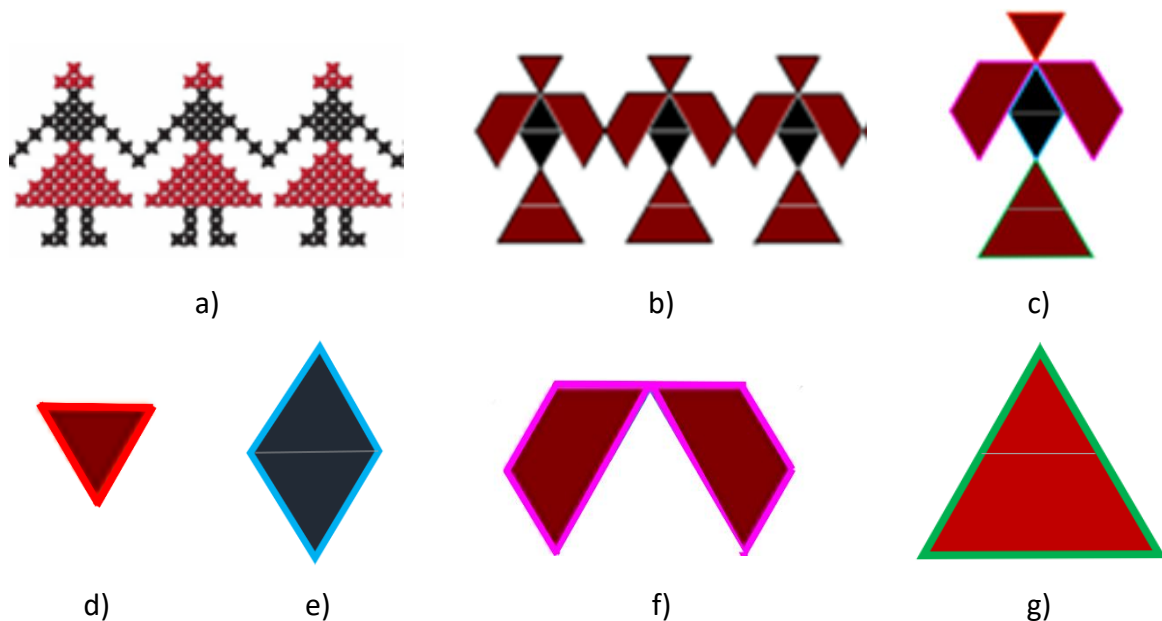
Fig. 2.11. a. Traditional Romanian model; b. Project translated into thermal solar facades for buildings; c. STC Assembly; d.Subassembly „eL";e. Subassembly „2t"; f. Two trapeze in contact; g. Subassembly „eL".

Based on the concept presented in the previous section, different applications can be generated such as:

- solar thermal facades with traditional design elements (Fig. 2.11);
- solar thermal facades with pseudo 3D (Fig. 2.12);
- solar thermal facades with stylized images (Fig. 2.13).

| a) | b) | c) | d) |

| e) | f) | g) | h) |

| i) | j) |
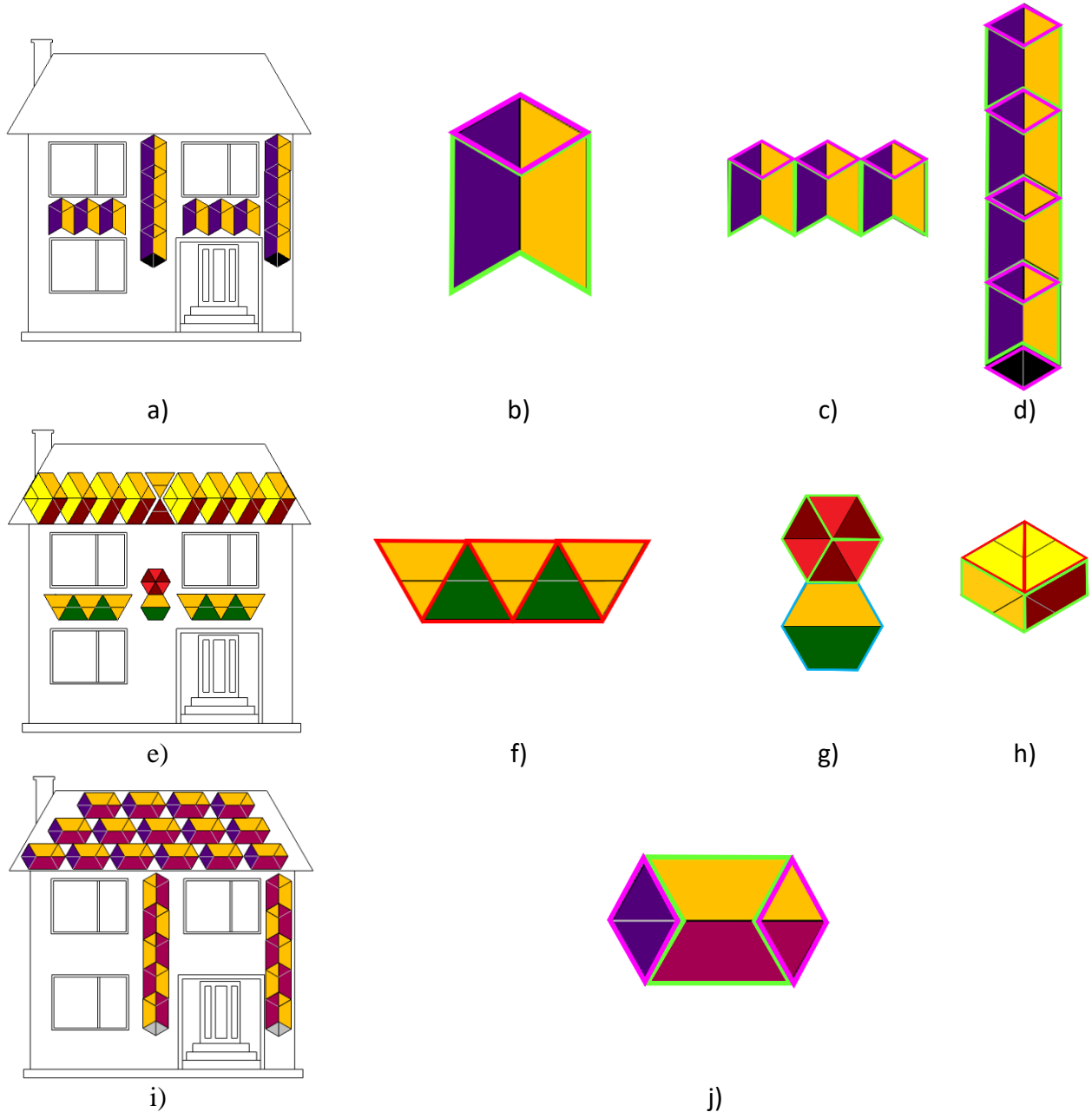
Fig. 2.12. Pseudo 3D thermal solar collectors installed on the facades and roof of the building (a,e,i) and representation of assembly and subassemblies from two collectors used (b-d;f-h, j)

Various designs are possible, and coverage can be increased by installing more unconventional collectors as in Fig.2.12, both on the facade and on the roof. Fig.2. 12.a includes a set of collectors arranged in the form of columns; they are formed by subassemblies of 2 trapezoidal and triangular collectors as follows: **,,bb”**- marked with green

and **„ee"** – with pink in Fig.2. 12.b. Several subassemblies of this type arranged in series form an image similar to a fan or a fence (Fig.2. 12.c), respectively, arranged vertically give the impression of a column (Fig.2. 12.d). Contrasting colors give the impression of light and shadow to the formed images.

a)

b)

c)

d)

e)

f)

g)

h)

i)
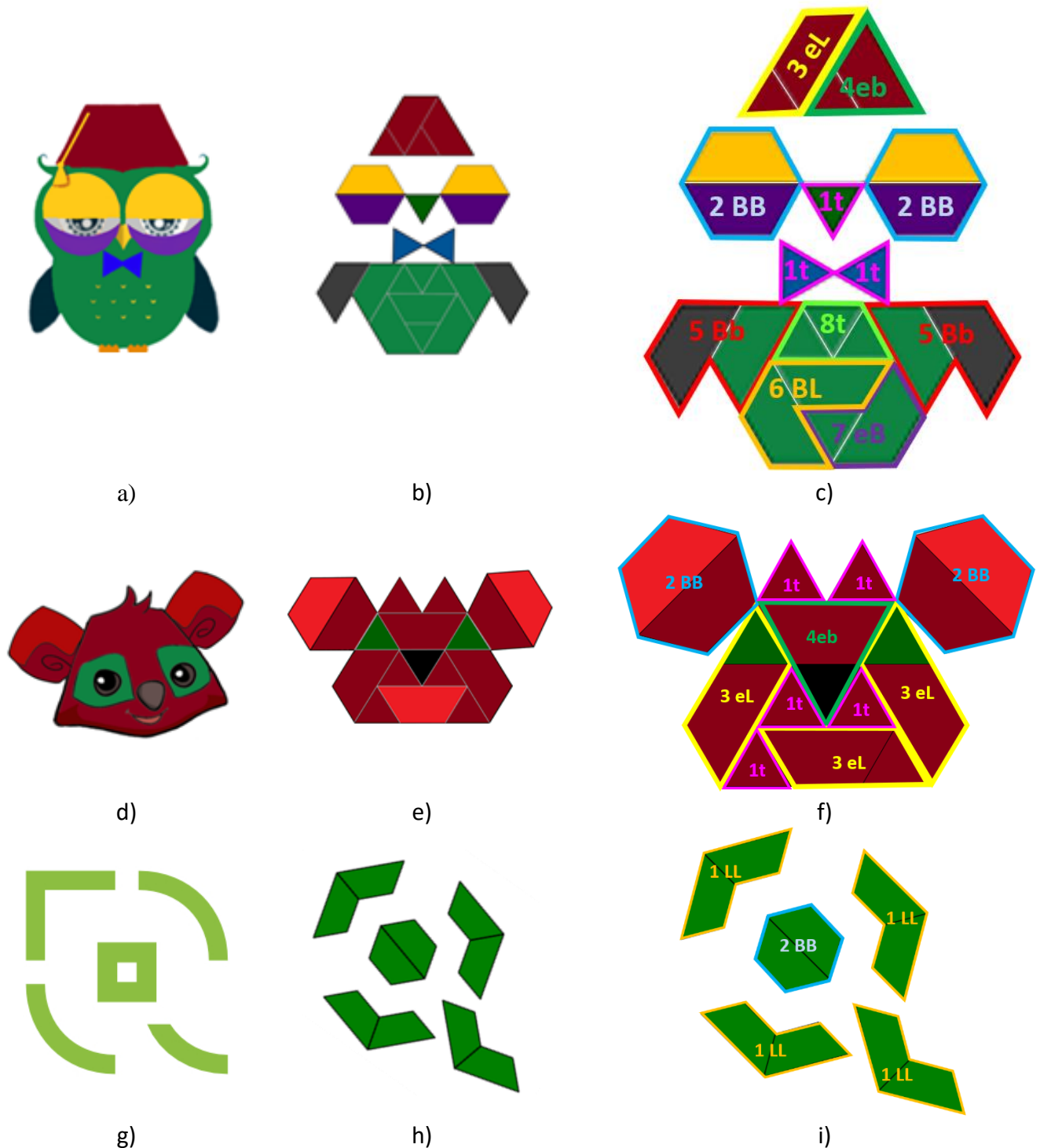
Fig. 2.13. Stylized images for thermal solar facades: a) Owl; b) The koala bear;
c) Logo of the Faculty of Product Design and Environment of
Transilvania University of Brașov

In Fig.2. 12.e. another design arranged on the facade and roof is represented. On the facade of the building, the trapeze and triangle STC were arranged in the form of a flower (Fig. 2. 12.f) made of the subassemblies *„BB"* (outlined in blue) and 3x *„2t"* (outlined in green); and two other groups of collectors (Fig.2.12.f) consisting of 5 type subassemblies *„eb"*, marked in red, they can be likened to blades of grass. On the roof of the building there are 2 rows formed by the assembly represented in Fig.2.12.h. which is made up of 2x *„eb"* outlined in red, respectively 2x *„eL"* outlined with green; and in the center of the two strings are 2 type subassemblies, *„eb"* arranged in a mirror, vertically to imitate an hourglass.

In Fig.2.12.i. the same assembly from 2.12.b is used, to which one more type subassembly is connected *„ee"* outlined with pink (Fig.2. 12.j). Thus, the model represented on the roof is arranged in the form of attic windows, while the columns on the facade give the impression of brick columns due to the chosen cherry color.

Triangular and trapezoidal solar thermal collectors and their sub-assemblies can be used for the stylized representation of varied and complex images. For example, in Fig. 2. 13.a., b. an owl is represented, for which the following units/subassemblies were used (Fig.2. 13.c): 3x *„1t"* (pink), 2x **2-*„BB"*** (blue), **3-*„eL"*** (yellow), **4-*„eb"***(green)**,** 2x **5-*„bB"*** (red)**, 6-*„BL"*** (orange)**, 7-*„eB"*** (purple) și **8-*„3t"***. A koala bear head is stylized in Fig.2. 13.d., e. to which it has been used: 5x *„1t"* (pink), 2x **2-*„BB"***(blue), 3x **3-*„eL"***(yellow) și un **4-*„eb"***(green) (Fig.2. 13.f). The logo of the Faculty of Product Design and Environment, from Transilvania University in Brașov is represented in Fig. 2.37.g.,h. from: 4x **1-*„LL"*** (yellow) and 1x **2-*„BB"*** (blue) (Fig.2. 13.i).

3. Study of the thermal behavior of the triangular flat solar collector with serpentine

3.1 Description of the collector

The existing triangular-shaped solar thermal collectors (Vișa et.al., 2017) have a cavity inside for the circulation of the thermal agent, and in the trapezoidal ones, the fluid circulation is carried out through the serpentine. To facilitate the joining of the two forms, it is necessary to adapt one of the collectors to the design of the other. It is proposed for the development of a flat triangular solar thermal collector with serpentine, the dimensions of which correspond to the dimensions of the existing trapeze.

Table 3.1. Basic configuration of the STC concept

The edge of the triangular thermal solar collector	L_{CST}	750 mm
The thickness of the triangular solar thermal collector	G_{CST}	82 mm
The thickness of the air layer	G_a	10.4 mm
Aperture edge	L_a	650 mm
The thickness of the rear thermal insulation	G_p	50 mm
The thickness of the lateral thermal insulation	G_L	20 mm
Glass thickness	G_s	4 mm
Absorbent plate thickness	G_{pa}	0.4 mm

The constructive parameters of the collector are represented on the triangular thermal solar collector in Fig.3.1.a, and in Fig.3.1.b the component elements are represented in an isometric view. Each constructive element is taken into account in the studied model, for its dimensioning, in order to obtain an optimal flat triangular thermal solar collector. To facilitate the connection of the CST with a second unit of the same shape or of a trapezoidal shape, the serpentine variant with the outlet on the side of the solar thermal collector is proposed.

The triangular STC concept with serpentine includes: a metal casing made up of two frames: front (1) with the related space dedicated to the solar glass (3), and respectively the rear frame (9) which will support the rest of the component elements; to minimize thermal losses, thermal insulation is needed both on the side (7) and on the rear level of the collector (8); the main element, the STC serpentine (6), will imitate the triangular shape of the frame and will be glued to the absorbent plate (5) for better thermal transfer; spacer (2,4) is needed to support the absorber and to keep the distance between the glass and the absorber constant.

Starting from the basic version described previously, through analytical modeling and numerical simulation of the thermal behavior of the collector, under the conditions of keeping the overall dimensions that ensure assembly with an existing trapezoidal collector, the optimal version of the collector is developed which will later be experimentally tested.
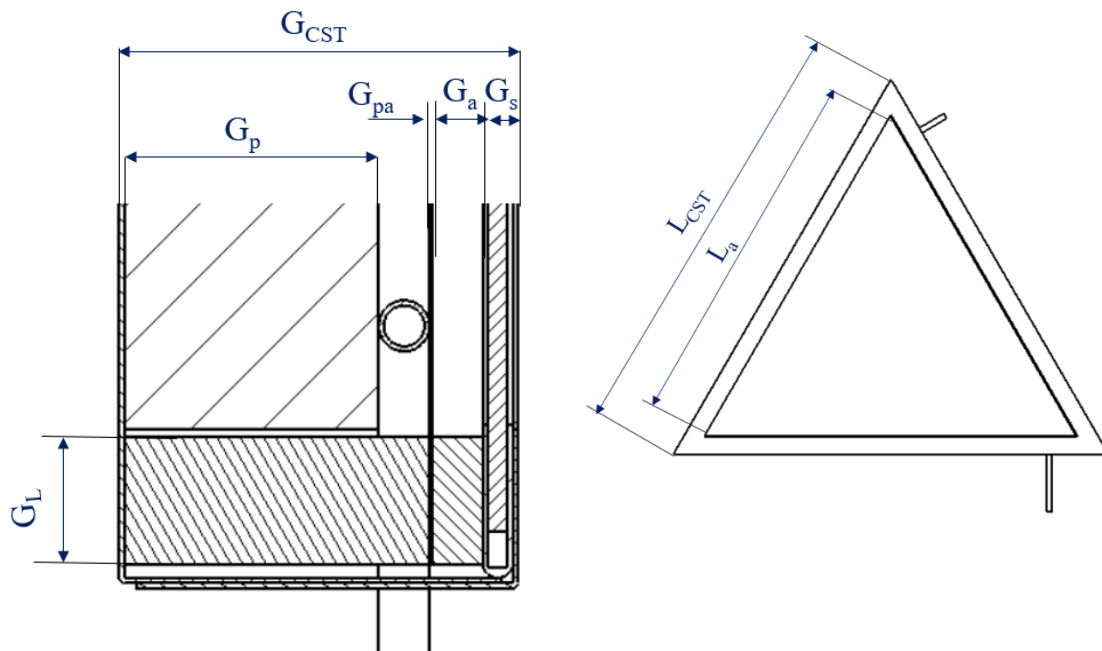
Fig. 3.1.a. Constructive parameters of the triangular flat solar thermal collector

Summary	5- Absorber plate
1- Frontal frame	6- Serpentine
2- Spacer	7- Lateral thermal insulation
3- Glass	8- Posterior thermal insulation
4- Spacer	9- Posterior frame
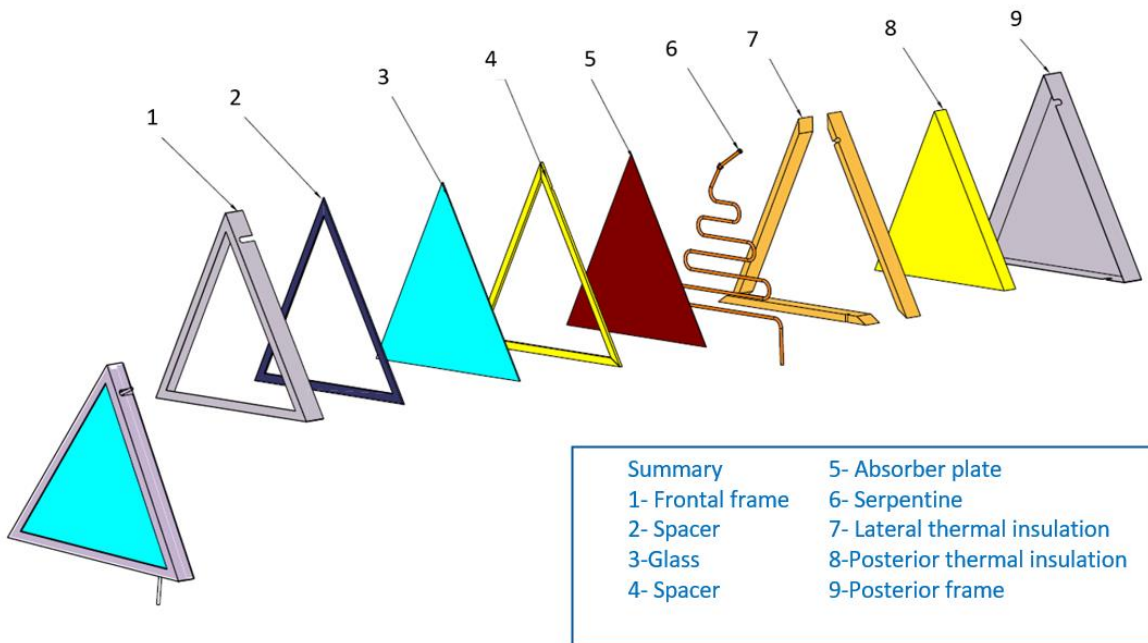
Fig.3.1.b. Conceptual variant with each element in isometric view

3.2 Heat losses through thermal transfer

In the thermal solar collector, losses occur through heat transfer through conduction, convection and radiation, at the front, back and side level (Fig. 3.2). The required thermal energy is obtained as a result of the heat transfer between the absorber and the pipes. Based on them, the thermal efficiency of the triangular thermal solar collector, with black and red absorbers, is calculated, adapting the model proposed by Duffie and Backman (Duffie & Backman, 2006) to the studied triangular STC.

Total thermal losses (U_t) represents the sum of all heat transfer losses at the frontal level (U_f), posterior (U_p) and lateral (U_L) of the triangular plan-flat solar thermal collector estimated under the ambient conditions and has the following relationship:

$$U_t = U_f + U_p + U_L \qquad [W/m^2°C] \qquad (3.1)$$

where:
U_f – represents the frontal losses by convection and radiation;
U_p – represents the posterior conduction losses;
U_L – represents lateral convective and conductive losses.
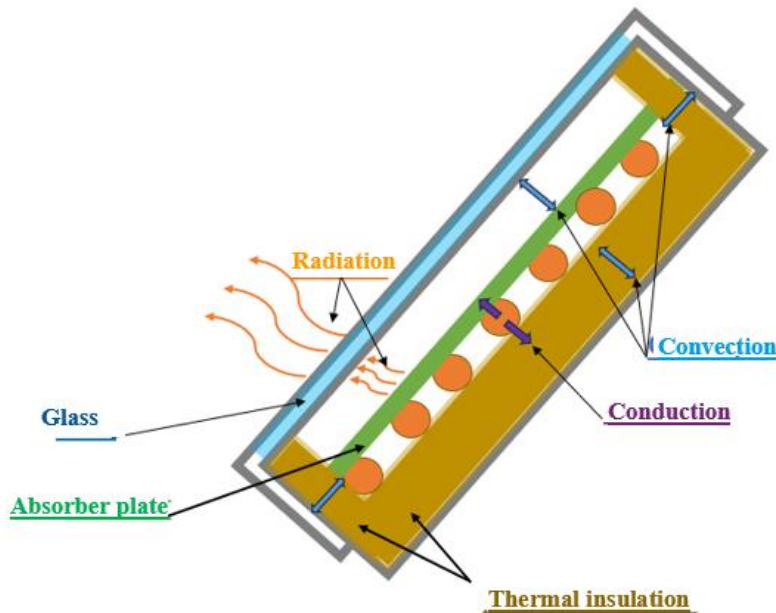
Fig. 3.2. Frontal, posterior and lateral thermal losses of the triangular solar collector

The frontal heat losses are determined with:

$$U_f = \left(\frac{1}{h_{c,p-s}+h_{r,p-s}} + \frac{1}{h_v+h_{r,s-a}}\right)^{-1} \qquad [W/m^2°C] \qquad (3.2)$$

where:

$h_{c,p-s}$ – heat transfer coefficient by convection (c) between absorbent plate (p) and glass (s) , [W/m²°C];
$h_{r,p-s}$ – radiation heat transfer coefficient (r) between the absorber plate and the glass, [W/m²°C];

h_v – heat transfer coefficient caused by wind, [W/m²°C];

$h_{r,s-a}$ – heat transfer coefficient by radiation between the glass and the external environment, air (a), [W/m²°C].

The transfer coefficient caused by the influence of wind speed has the value $h_v = 5\ W/m^2$ for solar thermal collectors in the vertical plane under static conditions.

Coefficient of heat transfer by convection between the absorbent plate and the glass is determined with the relationship

$$h_{c,p-s} = Nu\frac{k}{G_a} \qquad [W/m^2°C] \tag{3.3}$$

where:

Nu – is number of Nusselt;

k – represents the thermal conductivity of the air [W/m²°C];

G_a – represents the thickness of the air layer [mm].

The radiation heat transfer coefficient between the absorbent plate and the glass surface is calculated by

$$h_{r,p-s} = \frac{\sigma(T_p^2 + T_s^2)(T_p + T_s)}{\frac{1}{\varepsilon_p} + \frac{1}{\varepsilon_s} - 1} \tag{3.4}$$

where:

$\sigma = 5.67 \cdot 10^{-8}\ W/m^2 \cdot K^4$ constant Stefan − Boltzmann;

T_p - is the average temperature of the absorber plate $[K]$;

T_s - is the estimated temperature of the glass surface $[K]$;

ε_p - is the thermal emittance of the absorber plate $[W/m^2]$;

ε_s - is the thermal emittance of the glass surface $[W/m^2]$.

Frontal radiation losses also occur between the glazed surface (solar glass) and the outside environment. The radiation transfer coefficient between the glass and the outside environment is

$$h_{r,s-a} = \varepsilon_s \cdot \sigma \cdot (T_s^2 + T_a^2)(T_s + T_a)\ [W/m^2\ {}^oC] \tag{3.5}$$

where:

ε_s – is the thermal emittance of the glass surface;

σ –constant Stefan − Boltzmann ;

T_a - ambient air temperature, $[K]$;

T_s – the temperature of the glazed surface. It is calculated according to the equation

$$T_s = T_p - \frac{U_t(T_p - T_a)}{h_{c,p-s} + h_{r,p-s}} \qquad [{}^oC] \tag{3.6}$$

The frontal heat losses by radiation between the absorbent plate and the glazed surface depend on the emissivity of the surface. The emittance is 0.95 for the black aluminum absorber plate and 0.88 for the transparent glass, respectively (Duffie and Backman, 2006). For other colors of selective surfaces, the values differ. Surfaces of different colors were studied to check their emittance and absorbance values, which were measured at different wavelengths – hence the difference between 2 similar colors (Table 3.2). Most of the colors are obtained by the technique of depositing thin layers. Spray paint was used to make the two absorbent plates, which was sprayed on the surface of the absorber in a uniform layer. The percentage values for black color absorbance are similar (table 3.2. rows 1, 10, 14, 16, 27) even when the technique used to obtain the color is different (sol-gel layer depositions vs. paint), the absorbance is 95%. For red, there are differences from one

technique to another, the shade of red being different, but according to studies carried out in the RESREC Research Center of Transilvania University (Isaac L. et.al., 2018) for red paint the absorbance is 53%, of such other studies show that for the red color the absorbance is between 50-90% depending on the technique and the shade obtained. According to Kirchhoff's law, under conditions of thermal equilibrium, the emittance is equal to the absorbance. Following the study, the values are chosen so they are close to the color used:

- **black α_n= 95%; ε_n= 0.95;**
- *red α_r= 60 %; ε_r=0.6.*

Table 3.2. Absorbance and emittance for different colors

No.	Color		α [%]	ε [%]	α/ε [%]	Reference
1	black paint		95	5	19	(Feiliang et.al., 2015)
2	red		95.3	4.3	22.2	
3	purple		97.6	4.5	21.7	
4	magenta		95.0	4.4	21.6	
5	mauve		95.2	4.5	21.2	
6	blue		95.5	4.7	20.3	
7	turquoise		95.3	4.4	21.7	
8	green		95.6	4.6	20.8	
9	brown		95.3	3.5	27.2	
10	dark colours		95	1	95	(Tripanagnostopoulos et.al.,2000)
11			85	5	17	
12	light colors		75	9	8.3	
13			65	9	7.2	
14	black		94.9	6.2	15.3	(Grosjean et.al., 2021)
15			91.4	9	10.2	
16	black epoxy		94-96	5-10	9.4-19.2	(Butler B.et.al.,1979)
17	purple		92.3	7.6	12.1	(Lai și Li,2022)
18	yellow		90.5	9.1	9.9	
19	light green		91.1	8.5	10.7	
20	dark green		93	7.3	12.7	
21	blue		93.2	7.1	13.1	
22	red-Fe_2O_3		65	7	9.3	(Duță et.al., 2014)
23	yellow - V_2O_5		53	14	3.8	
24	black- blue- CuS		69	20	3.5	
25	red paint		53	13	4.1	(Isac L. et.al., 2018)
26	red - Fe_2O_3 sol-gel		64-70	5-12	12.8-5.8	
27	black - NiS_x - sol-gel		84-95	41-52	2-1.8	
28	red		88	54	1.63	(Probst, Roecker, 2007)
29	cherry-colored		89	41	2.17	
30	red		82	27	3.03	(Wu Y. et.al.,2013)
31	red		50-70	50	1-1.4	(Engineering Tool Box)

Posterior thermal losses (U_p) it is carried out by convection and is calculated according to the thermal conductivity and the thickness of the posterior thermal insulation of the collector

$$U_p = \frac{k_p}{G_p} \qquad [W/m^2\ {}^oC] \qquad (3.7)$$

where,

k_p - the thermal conductivity of the insulating material $[W/m^2\ {}^oC]$;

G_p - the thickness of the rear thermal insulation $[mm]$.

For an extruded polystyrene thermal insulation, the thermal conductivity is 0.03 W/m²°C, and for mineral wool it is 0.45 W/m²°C.

Lateral thermal losses (U_L) of the solar thermal collector is achieved by convection and is calculated with the relation

$$U_L = \frac{(UA)_L}{A_a} \qquad [W/m^2\ {}^oC] \quad (3.8)$$

where:

(UA)$_L$ - represents the product between the coefficient of lateral thermal losses through thermal conduction and the lateral area of the solar thermal collector;

A_a – represents the aperture area of the thermal solar collector, [m²].

The coefficient of lateral thermal losses is equal to the ratio between the coefficient of conduction and the thickness of the lateral thermal insulation

$$U = \frac{k_L}{G_L} \qquad [W/m^2\ {}^oC] \quad (3.9)$$

Heat transfer efficiency between the absorber and the pipe is calculated according to the useful power transmitted through the pipes and the global solar radiation intensity captured by the absorber, with the relation

$$\eta = \frac{q}{A_a G_n} \qquad [\%] \qquad (3.10)$$

where:

q- is the useful thermal power resulting from the heat transfer between the absorber and the pipe, [J/s];

A$_a$ – is the aperture area, [m²];

G$_n$- is the intensity of the global solar radiation captured by the STC, [W/m²].

The useful power produced by the heat transfer between the absorber and the pipes is calculated with

$$q = A_a F_R \left[\tau \alpha G_n - U_t (T_p - T_a) \right] \ [J/s] \qquad (3.11)$$

where:

A$_a$ – is the aperture area , [m²];

F$_R$ – is the heat extraction factor;

τ – is the transmittance of the glass;

α – the absorbance of the color of the absorber plate of the thermal solar collector;

G$_n$ – is the intensity of the global solar radiation captured by the STC, [W/m²];

U$_t$ – represents the total thermal losses in the collector, [W/m²°C];

T$_p$ – is the temperature of the absorber plate, [°C];

T$_a$- is the air temperature, [°C].

The heat extraction factor is determined with the relation

$$F_R = F' \cdot F''$$ (3.12)

where:

F' - is the efficiency factor of the solar thermal collector;

F'' - is the flow factor of the thermal agent.

Because the intermediate factors used in the calculation of the efficiency of the solar thermal collector such as $\tau\alpha$, F_R, U_t și G_n has constant values, a simplified efficiency relationship can be formulated which will be used further to compare the calculated efficiency with experimental testing. Thus, introducing the relationship 3.11 in 3.10, and divided first term by G_n it is obtained:

$$\eta = \tau\alpha F_R - \frac{F_R \cdot U_t}{G_n}(T_p - T_a)$$ (3.13)

Heat extraction coefficient F_R depends mainly on U_t (total thermal losses in the collector) și C_p (the specific heat of the thermal agent used). The total thermal losses are calculated for the two collectors of different colors having the same constructive parameters, so it can be considered a constant value for each color separately. In contrast, specific heat is a property of the heat agent that depends on its temperature. For temperature differences of 0-40°C at which testing is performed, C_p has little influence on the factor F_R (Table 3.3):

Tabel 3.3. The parameters that influence the factor F_R

No. crt.	Color	U_t	Δt	C_p	F_R
1			0	4182	0.846
2			10	4180	0.847
3	negru	7.7	20	4178	0.848
4			30	4181	0.846
5			40	4184	0.848
6			0	4182	0.864
7			10	4180	0.865
8	roșu	6.6	20	4178	0.866
9			30	4181	0.864
10			40	4184	0.867

Since there are no large differences between the values, an average value of F_R is adopted: 0.847 for the black collector, respectively 0.865 for the red one.

The transmittance of a surface is its ability to allow solar radiation to pass through it. This determines how opaque or transparent a surface is.

The transmittance-absorbance product, $\tau\alpha$, it depends on the color of the absorbent pad. Absorbance values were noted previously (**0.95 for black, 0.6 for red**), and the **transmittance of the glass is 0.91** (Dupeyrat P. et.al., 2011). Thus, the transmittance-absorbance product is:

- **Black $(\tau\alpha)_n$ =0.86;**
- **Red $(\tau\alpha)_r$ =0.546.**

Thus, the product is considered $\tau\alpha\, F_R$ a constant denoted by "a" and the term $F_R \cdot U_t$ denoted by "b". The difference between the average temperature of the absorbent plate and the air temperature is denoted by Δt, and the efficiency becomes a function of average absorber and air temperatures::

$$\boldsymbol{\eta = a - \frac{b\Delta t}{G_n}}$$ (3.14)

The coefficients "*a*" and "*b*", they will have different values for the black and red absorbent plate, respectively, due to the different absorbance (0.95 black vs 0.6 red) which in turn causes different total heat losses. Also, the term "*b G_n*" has different values for indoor testing, where a constant value of is used G_n ; and for outdoor testing, where G_n is variable and is measured under clear sky conditions.

This will be used in chapter 4 to compare the simulated efficiency according to the literature method (Duffie&Backman) vs. formula adapted in this chapter and then comparing the simulated results vs. those obtained experimentally.

The efficiency of the triangular flat plan solar thermal collector can be calculated for the outdoor simulation according to Meliss' formulation (Meliss și Kleemann, 1993)

$$\eta = \frac{P_{out}}{P_{in}}100 \quad [\%] \tag{3.15}$$

where:
P_{out} – represents the useful thermal power of the solar thermal collector, [*W*];
P_{in} – the thermal power captured at the surface of the collector, [*W*].

Thermal power output, *P $_{out}$* is calculated with the relation

$$P_{out} = P_t = \dot{m} \cdot c \cdot (T_{out} - T_{in}) \quad [W] \tag{3.16}$$

where,
$\dot{m}$ – is the flow rate of the thermal agent, [*kg/s*];
c - is the specific heat capacity of water of 4186 [*J/(kg·K)*];
T_{out} – the temperature of the thermal agent at the outlet of the collector,[*°C*];
T_{in} – the temperature of the thermal agent at the outlet of the collector,[*°C*].

Input thermal power, also called solar power (P_s), is calculated with the relation

$$P_{in} = A_c \cdot G_n \quad [W] \tag{3.17}$$

where:
A_c – is the area of the solar thermal collector, [*m²*];
G_n – is the intensity of solar radiation captured in the plane STC, [*W/m²*].

Thus, the efficiency of the collector becomes
$$\eta = \frac{P_t}{A_c \cdot G_n} \quad [\%] \tag{3.18}$$
In the case of outdoor testing, the global solar radiation intensity available in the CST plane is calculated based on the Meliss mathematical model

$$G_n = B_n + D_n \; [W/m^2] \tag{3.19}$$

where:
B_n - is the intensity of direct solar radiation in the plane of STC, $[W/m^2]$;
D_n - is the intensity of diffuse solar radiation in the plane of STC, $[W/m^2]$.

Intensitatea radiației solare directe în planul CST se calculează după formula

$$B_n = B \cdot cos v \quad [W/m^2] \tag{3.20}$$

where,
B - is the intensity of direct solar radiation, $[W/m^2]$;
v - is the angle of incidence, [°].

The intensity of diffuse solar radiation is calculated with the following relationship:
$$D_n = D_h(1 + \sin \alpha)/2 \quad [W/m^2] \tag{3.21}$$
where D_h - is the diffuse radiation in the horizontal plane.

The difference between the numerically simulated efficiency and the real one resulting from indoor and outdoor testing results in the relative error (RE), which is equal to:
$$RE[\%] = \frac{|\eta_s - \eta_e|}{\eta_s} \times 100 \ [\%] \tag{3.22}$$

where:
η_s – is the numerically simulated efficiency [%];
η_e – is the experimentally derived efficiency [%].

3.3 Numerical calculation of thermal losses

Through the numerical calculation of the thermal losses and the efficiency of the collector and the modification of the constructive parameters of the initial configuration within constructively possible limits, the size and meaning of the influence of the constructive parameters on the thermal losses and the efficiency of the triangular CST is determined. This allows determining the optimal configuration of the triangular CST, which will be the basis for the development of the constructive solution, the realization of the physical model and its testing.

For the basic version with black absorber:
a. The calculated frontal losses represent 6,36 W/m²°C.

Table 3.4. Frontal thermal losses for the base model

No. Crt.	Iterations	G_a	$T_{s.estimated}$	$T_{s.calculated}$	$h_{c,p-s}$	$h_{r,p-s}$	$h_{r,s-a}$	U_f
		m	°C	°C	[W/m²°C]	[W/m²°C]	[W/m²°C]	[W/m²°C]
1.	1	0,0104	35,00	46,65	2,82	7,60	5,16	6,17
2.	2	0,0104	46,65	46,96	2,82	7,97	5,48	6,36
3.	3	0,0104	46,96	46,97	2,82	7,98	5,49	6,36
4.	4	0,0104	46,97	46,97	2,82	7,98	5,49	**6,36**

b. Lateral losses for a thermal insulation of 20 mm of mineral wool, have the value of 2,31 W/m²°C.

Table 3.5. Lateral losses for the base model

Nr. Crt.	G_L	k_L	U	P_{CST}	A_{CST}	A_a	U_L
	m	W/m²°C	W/m²°C	m	m²	m²	W/m²°C
1.	0,02	0,045	2,25	2,25	0,18	0,18	**2,31**

c. Posterior losses, having a thermal insulation of 50 mm of mineral wool, represent 0,9 W/m²°C.

Table 3.6. Posterior losses for the base model

No.	k_p	G_p	U_p
Crt.	W/m²°C	m	W/m²°C
1.	0,045	0,050	**0,90**

From these calculations, the total thermal losses results, U_t, de 9.64 W/m²°C.

To determine the variation of the frontal losses, U_f, depending on the thickness of the air layer between the absorbent plate and the glass, the variation of this parameter from **0.005 m to 0.030 m** is considered. It resusts that once the distance between the absorbenr plate and the glass increases, thermal losses at the frontal level of the triangular STC decrease.
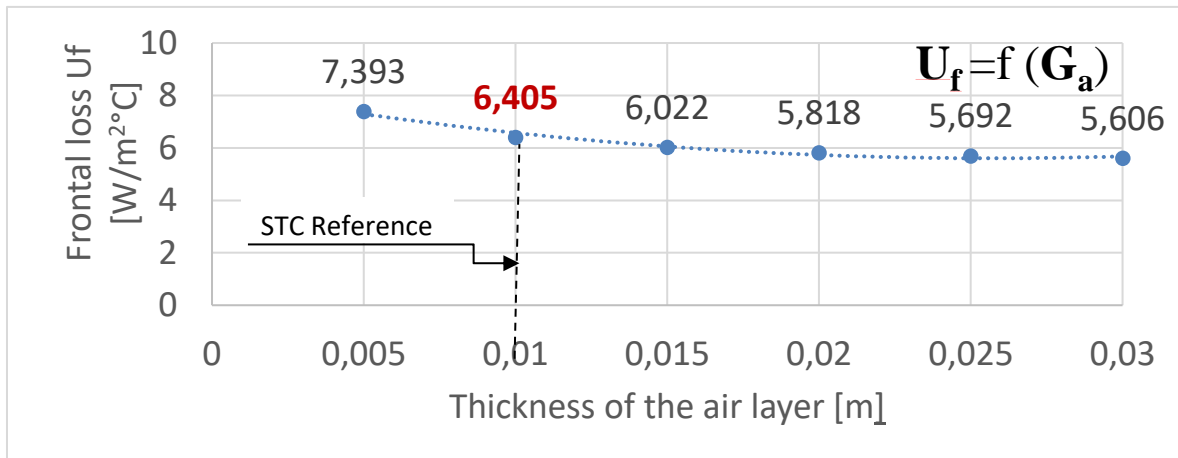
Fig.3.3. Graphic representation of the influence of air layer thickness on frontal heat losses.

Rear thermal losses are determined according to the thickness of the rear thermal insulation. To determine its influence, a variation of 5 mm starting **from 5 mm to 60 mm** is considered. The influence of thermal losses decreases with the increase in the thickness of the thermal insulation.

Fig.3.4. Graphical representation of the influence of thermal insulation thickness on posterior heat losses

To determine the influence of the thermal insulation thickness on the U_L level, the air layer thickness of 10.4 mm is considered constant, and the thermal insulation thickness varies **from 5 mm to 60 mm**. Fig.3.5 shows a major influence of the thickness of the lateral thermal insulation on the lateral thermal losses, which decrease as the thermal insulation increases.
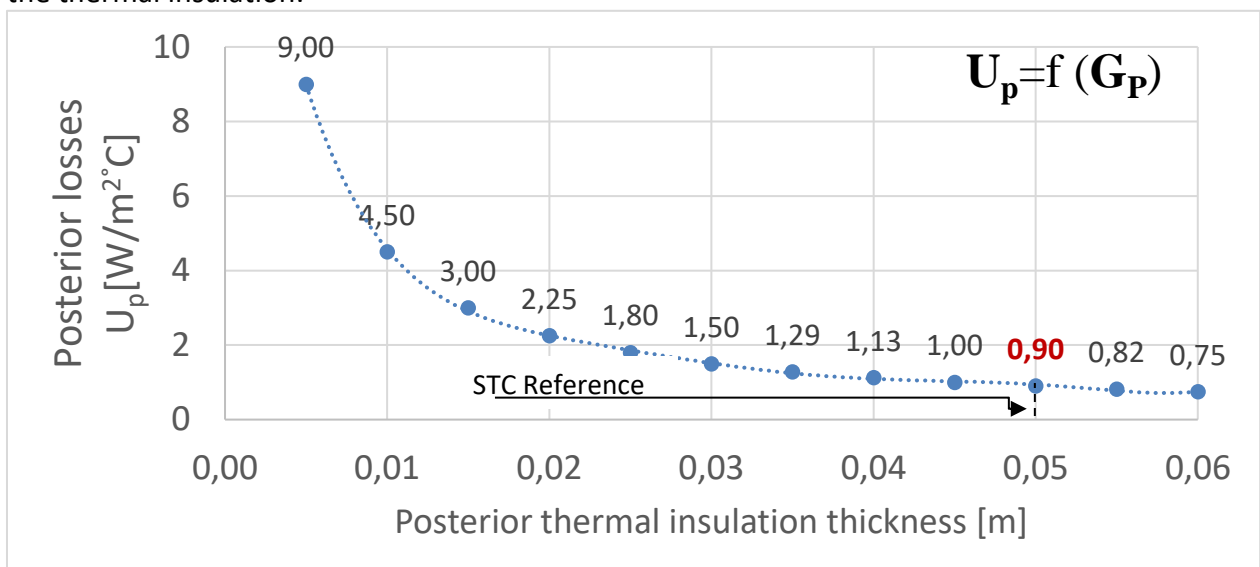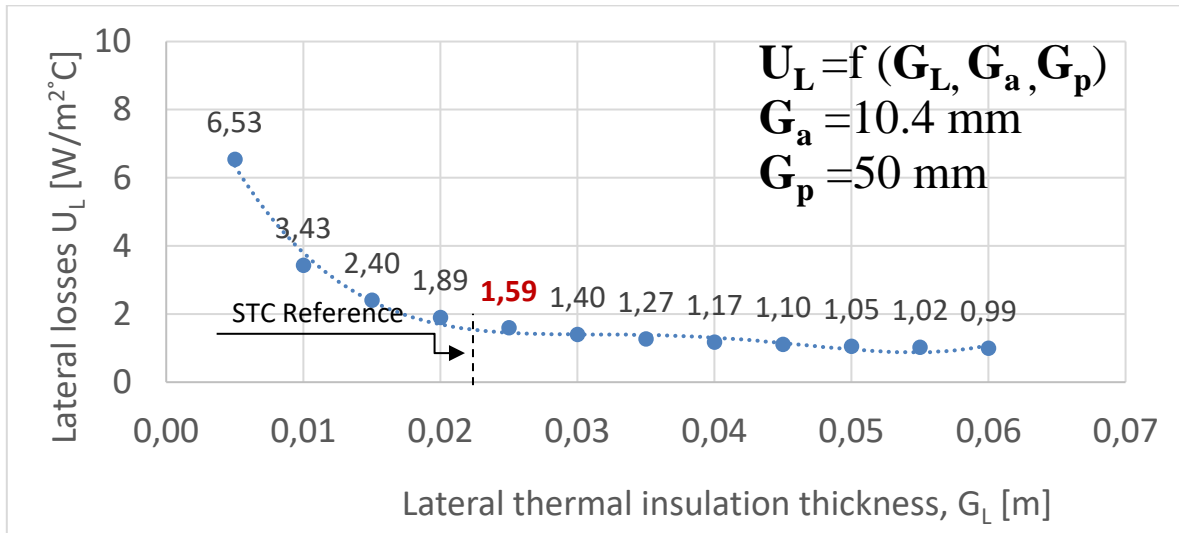

Fig.3.5. Graphic representation of the influence of the thickness of the lateral thermal insulation in the lateral thermal losses

To determine the influence of each parameter, the total thermal losses are calculated according to the thickness of the air layer, of the rear and side thermal insulation. The constant parameters are considered: the thickness of the air layer and of the rear thermal insulation - from which the constant frontal and rear thermal losses result; and the thickness of the lateral thermal insulation is varied from 5 mm to 60 mm, as well as the lateral thermal losses. Thus the variation of total thermal losses is obtained depending on the thickness of the lateral thermal insulation. The data is put in matrix form, representing the first row of Fig. 3.6. The influence of the parameters in the total losses is thus determined, forming the matrix form represented graphically. The calculation example for the first line in Fig.3.6 is represented in table 3.8.

On row no. 1, the total thermal losses are calculated for the air thickness of 0.005 m and the rear thermal insulation thickness of 0.005 m, for each side thermal insulation thickness starting from 0.005 to 0.06 m as follows:

$$U_t = U_f + U_p + U_{L\,(G_L = 0.005\,m)} = 7.4 + 9 + 6.53 = 22.93\ W/m^2°C$$

The total thermal losses are calculated according to each constructive parameter analyzed to observe their influence. In order to determine the influence of each parameter, a calculation matrix is required from which the graphic representation of the influence on the total losses results, according to Fig. 3.6.

This example is represented for the thickness of the air layer of 5 mm, with the variation of the back and side thermal insulation thicknesses. For each value of Gp varied, it results for each value of G_L varied, a specific value for the rear and side heat losses, respectively; cumulating them with the frontal losses related to G_a of 5 mm results in the total thermal losses.

Table 3.7. Algorithm for calculating total thermal losses

No.	G_a	G_p	G_L	U_f	U_p	U_L	U_t
-	m	m	m	W/m²°C	W/m²°C	W/m²°C	W/m²°C
1	G_{a1}	G_{p1}	G_{L1}	U_{f1}	U_{p1}	U_{L1}	U_{t1}
			G_{L2}			U_{L2}	U_{t2}
			...			...	...
			G_{Ln}			U_{Ln}	U_{tn}
2	G_{a1}	G_{p2}	G_{L1}	U_{f2}	U_{p2}	U_{L1}	U_{t1}
			G_{L2}			U_{L2}	U_{t2}
			...			...	...
			G_{Ln}			U_{Ln}	U_{tn}
...	...		...	...	...	...	...
n	G_{an}	G_{pn}	G_{L1}	U_{fn}	U_{pn}	U_{L1}	U_{t1}
			G_{L2}			U_{L2}	U_{t2}
			...			...	...
			G_{Ln}			U_{Ln}	U_{tn}

Table 3.8. The matrix form corresponding to the thickness of the air layer of 5 mm.

| G_a = 5 mm											
G_L → / G_p ↓	5	10	15	20	25	30	35	40	45	50	55	60
U_t											
5	22.9	19.8	18.8	18.3	18.0	17.8	17.7	17.6	17.5	17.5	17.4	17.4
10	18.4	15.3	14.3	13.8	13.5	13.3	13.2	13.1	13.0	13.0	12.9	12.9
15	16.9	13.8	12.8	12.3	12.0	11.8	11.7	11.6	11.5	11.5	11.4	11.4
20	16.2	13.1	12.0	11.5	11.2	11.0	10.9	10.8	10.8	10.7	10.7	10.6
25	15.7	12.6	11.6	11.1	10.8	10.6	10.5	10.4	10.3	10.3	10.2	10.2
30	15.4	12.3	11.3	10.8	10.5	10.3	10.2	10.1	10.0	10.0	9.9	9.9
35	15.2	12.1	11.1	10.6	10.3	10.1	9.9	9.9	9.8	9.7	9.7	9.7
40	15.1	11.9	10.9	10.4	10.1	9.9	9.8	9.7	9.6	9.6	9.5	9.5
45	14.9	11.8	10.8	10.3	10.0	9.8	9.7	9.6	9.5	9.5	9.4	9.4
50	14.8	11.7	10.7	10.2	**9.9**	9.7	9.6	9.5	9.4	9.4	9.3	9.3
55	14.7	11.6	10.6	10.1	9.8	9.6	9.5	9.4	9.3	9.3	9.2	9.2
60	14.7	11.6	10.5	10.0	9.7	9.5	9.4	9.3	9.3	9.2	9.2	9.1
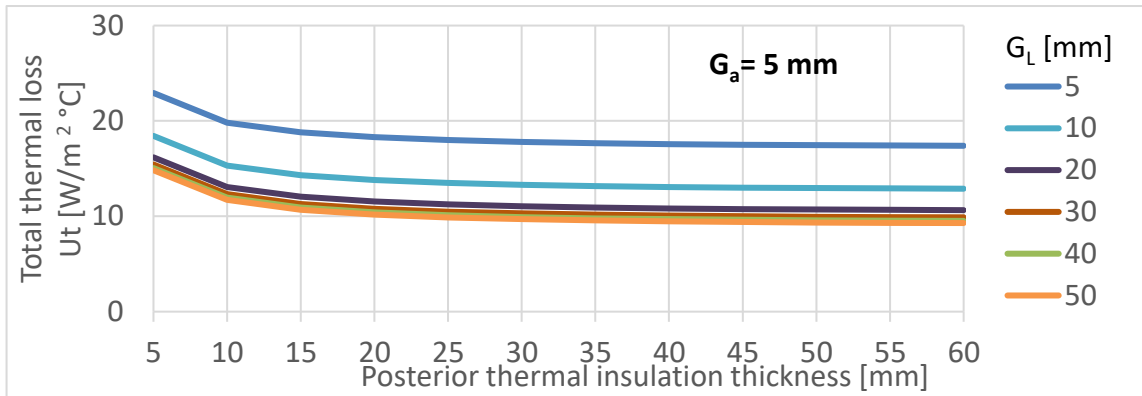
Fig. 3.6 The total thermal losses for the thickness of the air layer of 5 mm

The thermal energy transferred between the absorber and the pipes is influenced by the constructive parameters of the serpentine. They are identified in the following figure and represent:

- *W- the distance between two axes of two consecutive pipes;*
- *g - pipe wall thickness;*
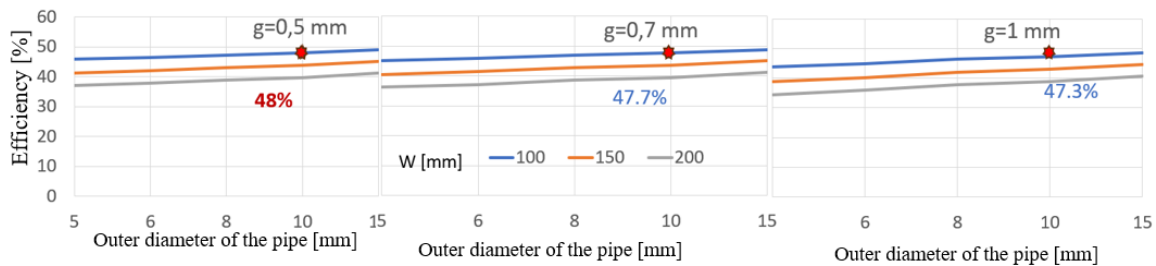- *D- the outer diameter of the pipe.*

Fig. 3.7. Triangular STC efficiency as a function of coil pipe dimensions

It follows that the higher efficiency is obtained for a small pipe distance of 100 mm for an outer diameter of 10 mm. The thickness of the pipe wall contributes to the increase in efficiency, but in a small percentage. Thus, an efficiency of 48% is obtained in the case of the thinnest pipe wall chosen for the calculations, of 0.5 mm. However, the influence of the pipe parameters is very small.

The efficiency of CST can also be influenced by the variation of the flow rate of the heating agent, but at higher than standard flow rates, the flow through the pipes becomes turbulent. Therefore, the value of the standard flow according to ASHRAED 109 will be used in the numerical simulations 0.02 kg/ m²s.

Numerically simulated efficiency

To compare the calculated numerical data with the test data, the simulated efficiency is determined in two cases, shown schematically in the figure 3.8:

1. *The intensity of global solar radiation captured by the collector is constant,* approx. 950 W/m², for comparing the simulated data with the indoor experiment in the chapter 4;
2. *The intensity of global solar radiation captured by the collector is variable*, for comparing the simulated data with the outdoor experiment, where G_n is calculated.

Finally, the two indoor and outdoor efficiencies will be compared and graphically represented.
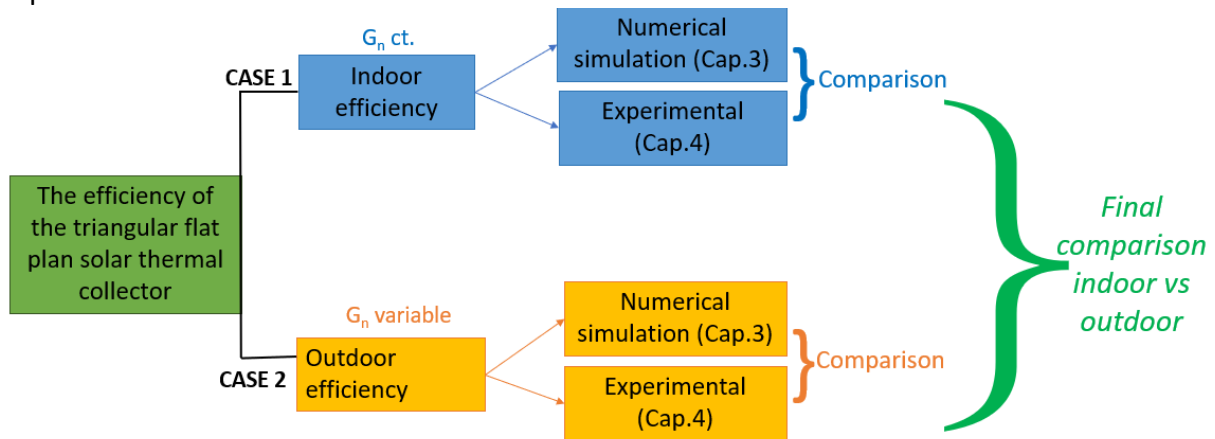

Fig.3.8. Schematic representation of the determination of the efficiency of the triangular flat solar thermal collector

Case 1: Indoor simulation: constant global solar radiation intensity approx. 950 W/m².

Figure 3.9 shows the numerically calculated efficiencies according to the model Duffie&Backman (η_{sin_N} for black STC and η_{sin_R} for red STC) with light bleu **73.143%** for black STC and with yellow for red STC of **43.004%.** And according to the noted simplified method $\eta_{(a,b)in\_N}$/$\eta_{(a,b)in\_R}$ and represented by navy blue and orange were obtained **73.21%** for black STC ($\eta_{(a,b)in\_N}$) and **47.04%** ($\eta_{(a,b)in\_R}$) for red. The two graphs overlap, the differences being very small **0.11-0.12 %.**

The STC efficiency is calculated according to the two numerical methods, and the coefficients related to the simplified method are presented in table 3.9 for the two colors of the absorbent plate (red vs. black).

Table 3.9. The efficiency calculated numerically by the two methods

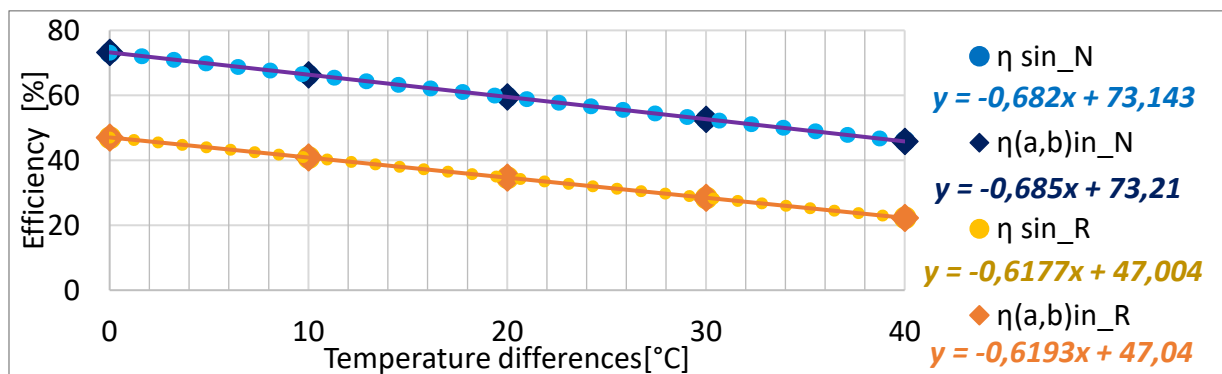| No.crt.	STC	a ($\tau\alpha F_R$)	$\tau\alpha G_n$	U_t	b ($F_R U_t/ G_n$)	$\eta_{(a,b)}$	η_{sin}	RE
		-	[W/m²]	[W/m²°C]	-	[%]	[%]	[%]
1.	Black	0.73	821	7.7	0.007	**73.21**	**73.143**	**0.12**
2.	Red	0.47	519	6.8	0.006	**47.04**	**47.004**	**0.11**

Fig.3.9. The simulated indoor efficiency for the black and red collector

Case 2: Outdoor simulation: variable global solar radiation intensity.

For the second case, the average values of the global radiation intensity captured by the collector are taken, calculated for 3 representative days in which the outdoor testing was performed (from chapter 4). As an example, it is represented graphically in fig. 3.10 intensity of global, diffuse and direct solar radiation from 31.12.2023 with $G_{n\ average}$ of 710 W/m^2 .
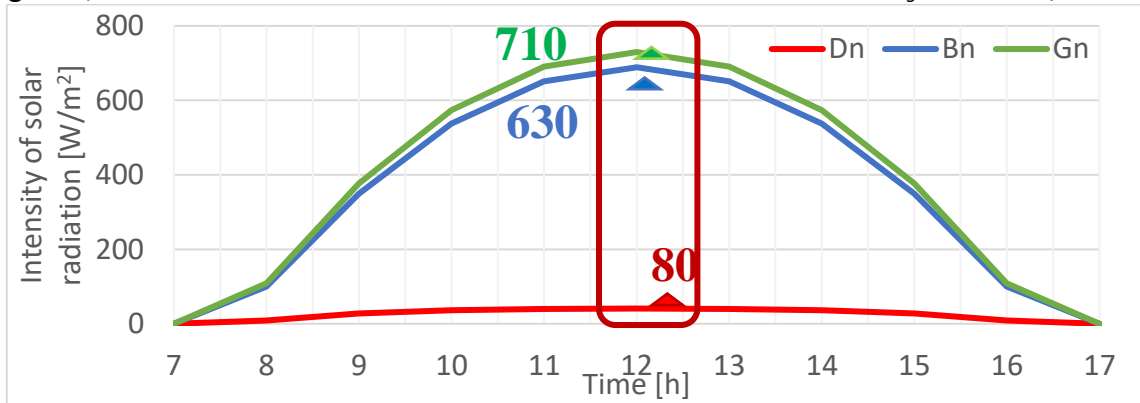

Fig. 3.10. Calculated solar radiation intensity for *31.12.2023*

Thus, for the 3 days, the following results of the CST efficiency simulated by the two methods are obtained (Table 3.10).

Table 3.10. Efficiency calculated numerically by the two calculation methods

No .crt.	a ($\tau\alpha\ F_R$)	Day	$\tau\alpha\ G_n$	U_t	b/ G_n =($F_R\ U_t$)/ G_n	η (a,b)out	η s out	RE
	-	-	[W/m^2]	[W/m^2°C]	-	[%]	[%]	[%]
1.	0.73 black	31.10.2023	651	7.7	0.0086	**73.2**	72.96	0.1
		13.11.2023	636		0.0088	**73.19**	73.14	
		31.12.2023	615		0.0086	**73.19**	73.14	
2.	0.47 red	31.10.2023	411	6.8	0.0078	**47.03**	46.04	
		13.11.2023	402		0.08	**47.03**	47	
		31.12.2023	388		0.0083	**47.03**	47	

The simulated results can be summarized graphically to compare the two cases indoor vs outdoor and for the two collectors with black and red absorber in Fig. 3.11. The simulations performed for the black collector are represented on the graph with green for indoor and blue for outdoor, and for the red collector the indoor ones are represented in pink while the outdoor ones are in red.
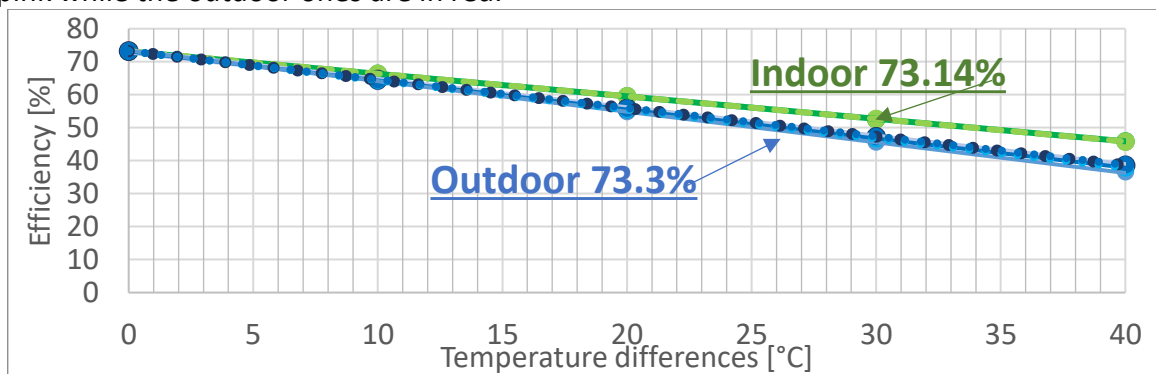
a.
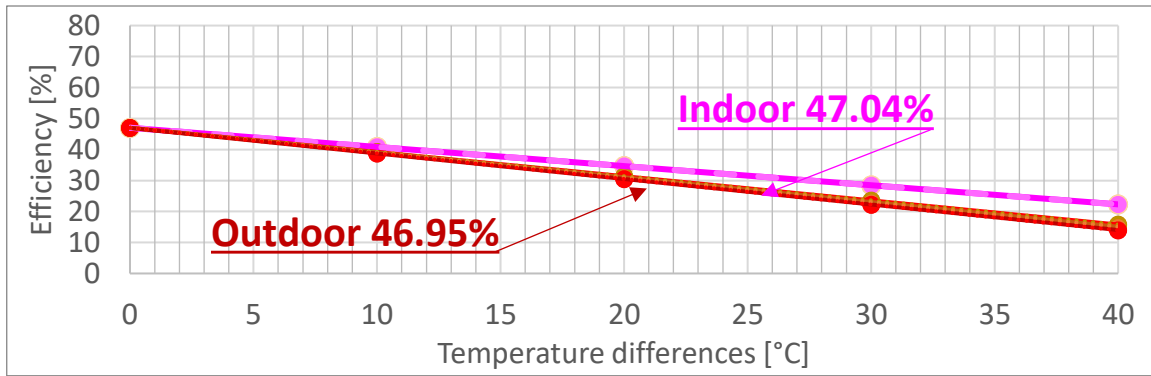
b.

Fig.3.11. Graphic representation of the comparison of indoor vs outdoor numerical simulations according to the two calculation methods for a. The black collector; and b. The red collector

Following the numerical simulations according to the classical Duffie&Backman method, they resulted:

- **in the case of indoor simulations, 73.14% were obtained for the black collector, and for the red one 47.004%;**
- **in the case of the outdoor simulations carried out for the three days (31.10, 13.11 and 31.12 2023) for black, results were obtained between 73.137-72.964%, and for red the results are 47.001-46.043%, for both collectors on the December day they are lower because the intensity of solar radiation is different compared to the other two days (710 W/m^2 vs 738/753 W/m^2).**

Following the numerical simulations according to the simplified method, it results:

- **in the indoor case, for the black collector 73.21%, respectively 47.04 % for the red one;**
- **in the outdoor case, for the black 73.193%, and for the red 47.03%.**

3.4. Dimensional-constructive design of the triangular collector with serpentine

As a result of the analysis, the main and secondary parameters resulted according to the following table, depending on their influence on the heat transfer and the efficiency of the collector:

Table 3.11. Constructive parameters of the flat solar thermal collector

No. Crt.	Parameter	Value [mm]	Category Principal	Category Secundar
1	The thickness of the air layer G_a	10	x	
2	Edge thermal insulation thicknesses G_L	25	x	
3	The thickness of the posterior thermal insulation G_p	50	x	
4	The thickness of the glass surface G_s	4		x
5	Absorbent plate thickness G_{pa}	0.4		x
6	The outer diameter of the pipe D	10		x
7	Pipe wall thickness g	0.5		x
8	The distance between two consecutive pipes W	60		x

The thermal solar collector is made of 1 mm thick aluminum sheet, with dimensions of 1000 x 2000 mm. To avoid waste of material, the cutting scheme of the sheet is made so that the two casings and the absorbent plate result from one sheet.
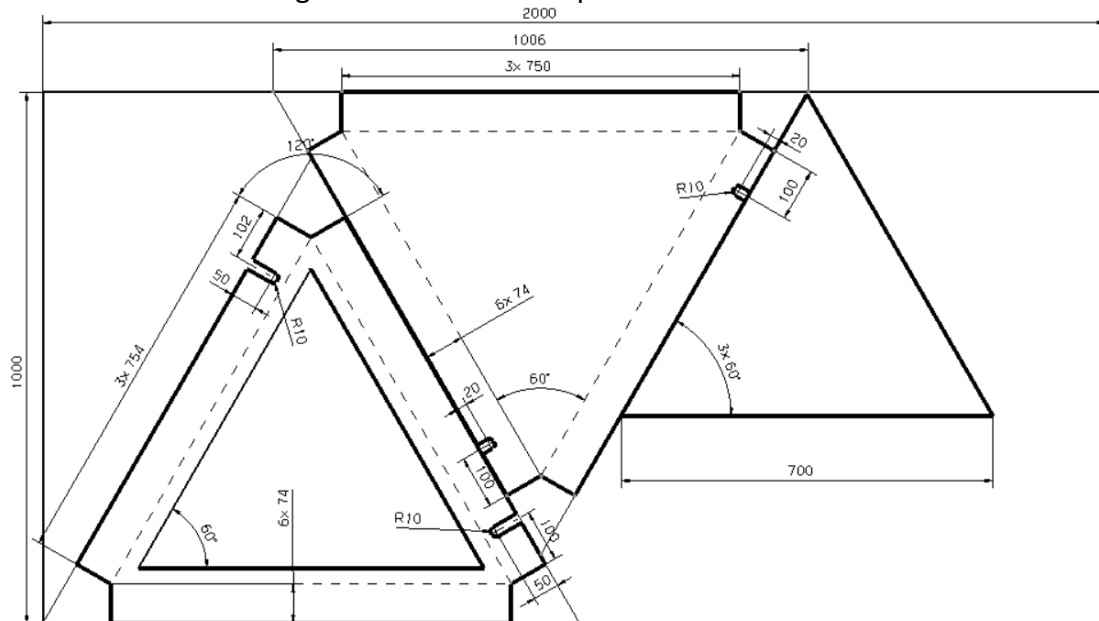

Fig.3.12. Sketch for efficient framing of shapes on a 2x1 m sheet of Al.

The serpentine is made of 10 mm diameter copper pipe with a wall thickness of 1 mm, forming 9 loops with a distance of 50 mm between two consecutive pipe axes. In total, it adds up to a length of approximately 3500 mm, it is represented according to Fig. 3.13.
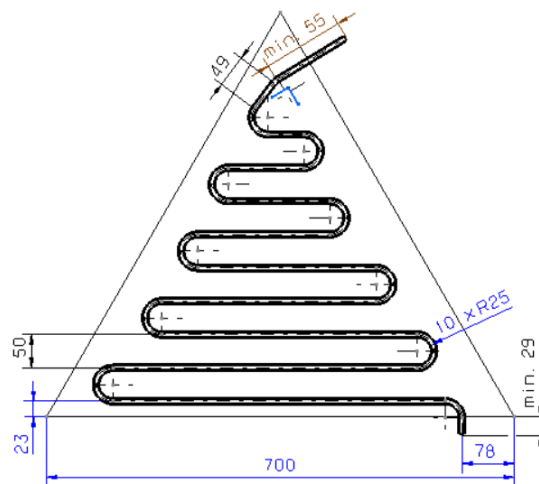
Fig.3.13 Technical drawing of the absorber plate with connected coil, front view

Thermal insulation is made of extruded polystyrene. 20 mm thermal insulation is used for the side of the collector, and 60 mm thick is used for the rear part.

Next, the steps followed in the construction of the optimal STC are presented:
1.   Marking of the aluminum sheet (Fig.3.14.1).
2.   Cutting out the frames (Fig.3.14.2).
3.   Bending the edges for the two frames (Fig.3.14.3).

4. Preparation of thermal insulation (Fig.3.14.4).
5. Preparation of the serpentine: (Fig.3.14.5).
6. Gluing the serpentine (Fig.3.14.6).
7. Painting the absorbent plate (Fig.3.14.7).
8. Gluing the glass (Fig.3.14.).
9. Cutting the holes for the inlet and outlet of the serpentine (Fig.3.14.9).
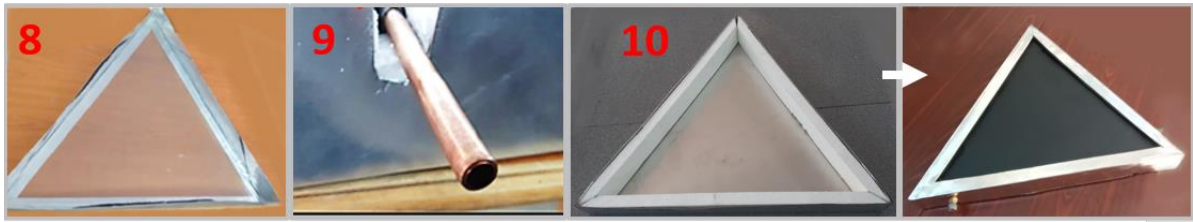10. Assembly of all components (Fig.3.14.10):

Fig.3.14. The construction stages of the flat triangular flat solar thermal collector
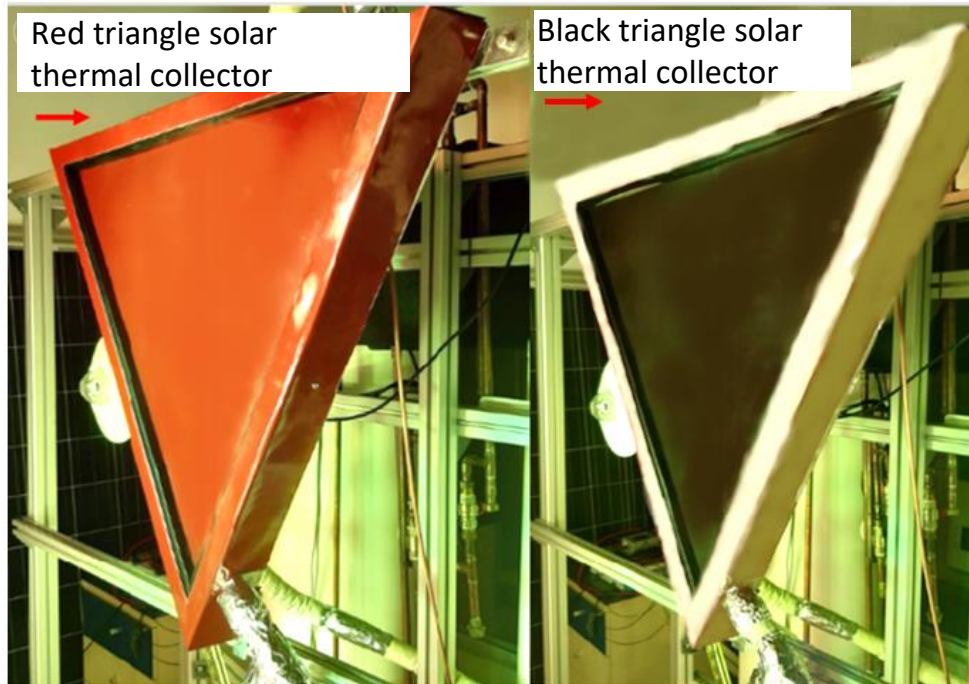

Fig.3.15. The triangular flat plan solar thermal collector with red and black absorber

After installing the collector on the stand, tests can be carried out under laboratory conditions.

4. Experimental testing of the triangular solar thermal collector with serpentine

The triangular coil solar thermal collector designed, modeled, studied and optimized in the previous chapters is physically developed and used for experimental validation of the thermal efficiency.

Fig.4.1. The two physical models of the red and black absorber plate collectors

Their testing is carried out using the existing stands in the RESREC Scientific Research Center of the Transilvania University Research and Development Institute (ICDT) in Brașov and adapted accordingly.

Experimental research is being developed on the indoor stand in laboratory conditions and on the outdoor stand in real conditions.

The graphical representation of the efficiency variation is done as a function of

$$\eta = f\left[(T_m - T_a)/G_n\right] \tag{4.1}$$

where

T_m - is the average temperature of the thermal agent, [°C];

T_a – is the air temperature, [°C];

G_n – is the global solar radiation intensity in the vertical plane of STC [W/m^2].

4.1. Indoor testing

Testing of solar thermal collectors is done according to ASHRAE standard 93-1996, which establishes specific test conditions such as: solar radiation level (900 ± 50 W/m^2), ambient temperature at the start of testing (25°C) and the temperature difference between the working fluid and the surrounding medium (10°C), hydraulic pressure of 2 bar and flow of 0,02 kg/m^{2}s (ASHRAE Standard, 1996). The temperature difference of the thermal agent at the entrance and exit of the solar collector is variable, divided into 5 steps as follows: ΔT = 0; 10; 20; 30; 40 °C.

The test stand is represented schematically in figure 4.2. and details in figure 4.3. It includes as main elements the thermal solar collector and the thermal energy tank, measuring devices for the flow or pressure of the heating agent, temperature sensors for monitoring the thermal parameters and valves for filling or evacuation of the circuit.

The components used in indoor testing are as follows:

a.   Main components:
1.   The solar simulator – which by means of UV lamps simulates the available solar radiation;
2.   Solar thermal collector – which transforms solar radiation into thermal energy, which it transfers to a thermal agent through the serpentine;

3. Storage tank - with the role of storing thermal energy. It also has an electrical resistance used as an additional heating source;
4. Hydraulic pump – with the role of ensuring the circulation of the thermal agent through the solar collector during testing, allowing the evaluation of its performance in real operating conditions;
5. Controller - which monitors the intensity of solar radiation;
6. The expansion vessel – to take over the increase in fluid volume after its heating and expansion;

b. Secondary components:
7. Fan/ wind simulator – used to cool the solar lamps;
8. Electric resistance – used to heat the boiler;
9. Flow meter – for measuring and monitoring the flow of the heat agent;
10. Manometer – for measuring hydraulic pressure in the system;
[G] Pyranometer – used to measure the intensity of solar radiation received by the collector. It is located near the collector, but without shading it;
[T] Temperature sensors - which have the role of measuring the temperature of the heating agent. They are located at the inlet/outlet of the heat agent from the collector and from the boiler, but also in the outside environment to monitor the air temperature;

c. Auxiliary components:
[DA] Automatic air vent - used to release the air from the solar thermal collector circuit installation;
SS The pressure valve - 10 bar - for releasing the pressure from the system in case it increases with the heating of the heating agent;
⋈ Valves for filling/emptying the installation;
〰 Flexible connections - through which the heat agent circulates.

Test procedure
Step 1. **Performing pressure tests.**
Step 2. **Connecting the CST system to the hydraulic system.**
Step 3. **Starting the hydraulic pump.**
Step 4. **Adjusting the flow rate.**
Step 5. **Placing the test stand in front of the vertical solar simulator.**
Step 6. **Adjusting the solar simulator.**
Step 7. **Checking the pyranometer and controller**

Monitored parameters:
- inlet and outlet temperature of the water from the solar thermal collector: T_{in}, T_{out};
- water temperature in the storage tank, T_b;
- ambient air temperature, T_a;
- simulated solar radiation intensity G_n;
- flow rate of the heating agent, $\dot{m}$;
- pressure in the solar circuit, p.

SUMMARY

G	Pyranometer
DA	Automatic vent
T	Temperature sensor for monitoring
⋈	Water tap
SS	Safety valve
AR	Cold water supply circuit
AC	Hot water supply circuit
〰	Flexible connections collector connection
—	Inlet circuit pipe
—	Outlet circuit pipe
-----	Monitoring circuit

10	Manometer	
9	Flowmeter	
8	Electric resistance for heating	
7	Wind simulator	
6	Expansion tank	
5	Controller for the solar circuit	
4	Hydraulic pump	
3	Tank/ storage	80 L
2	Triangular solar thermal collector	
1	Solar simulator	
Pos.	**Name**	**Obs.**

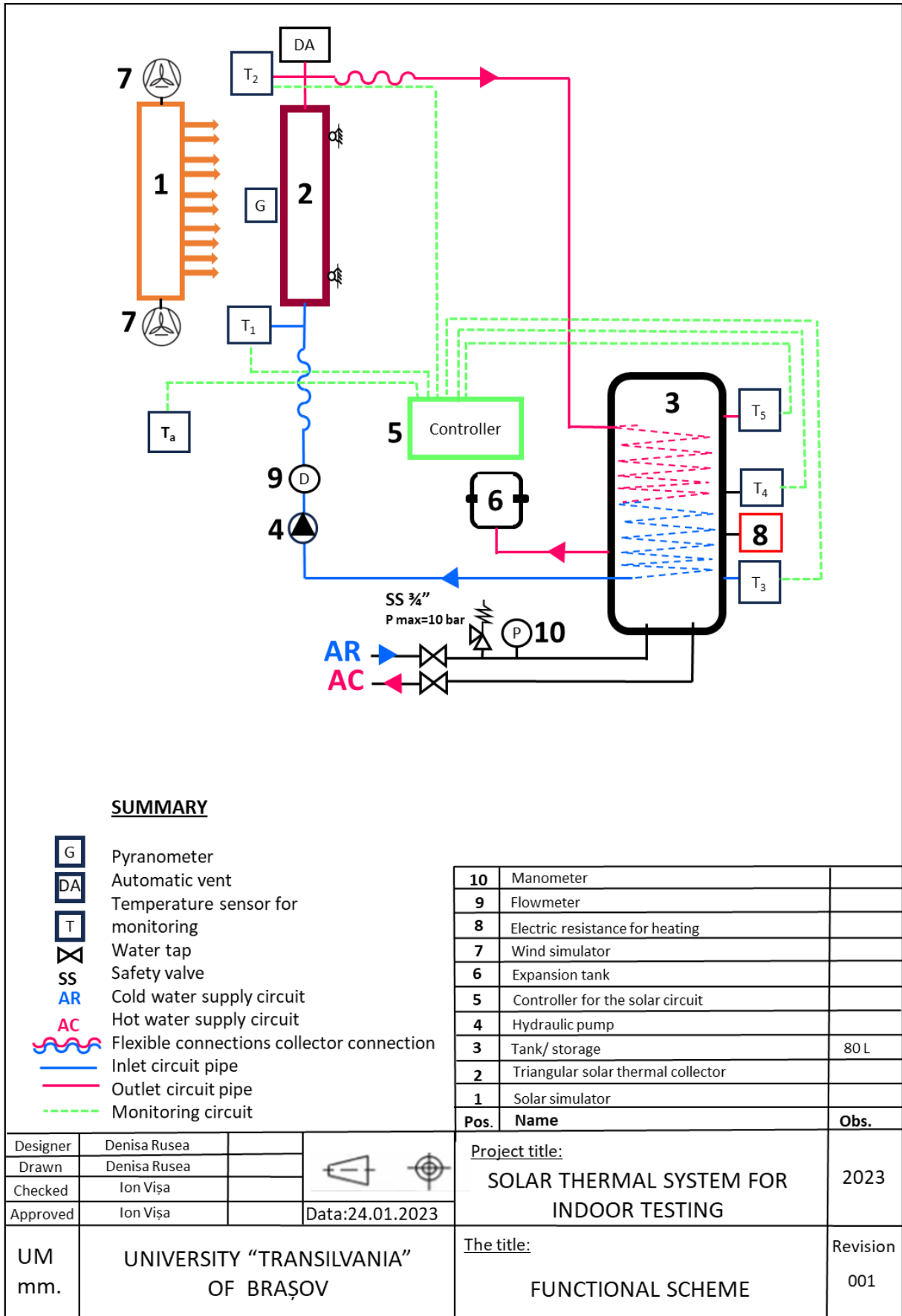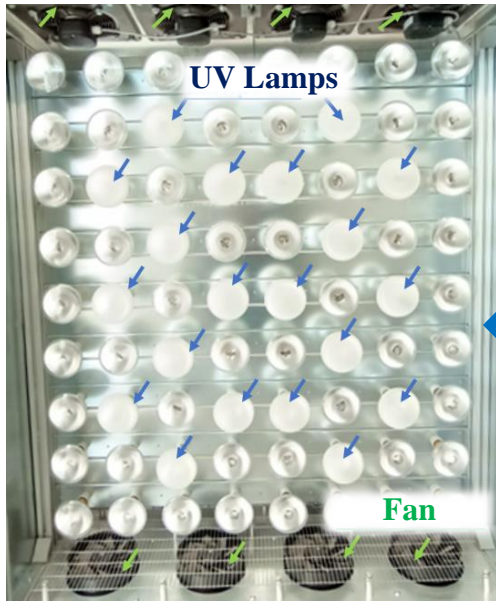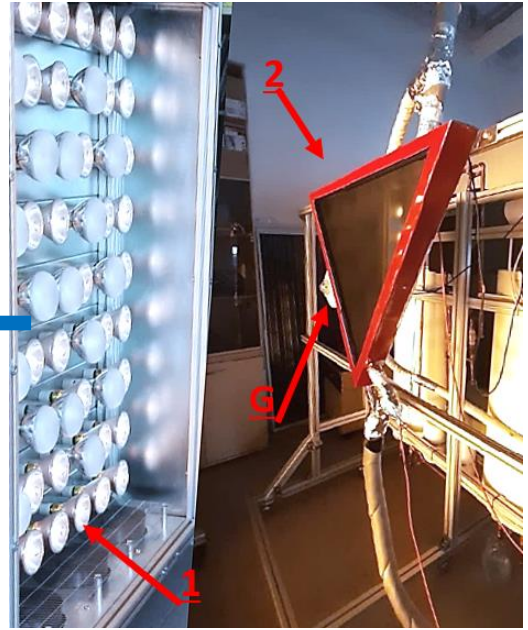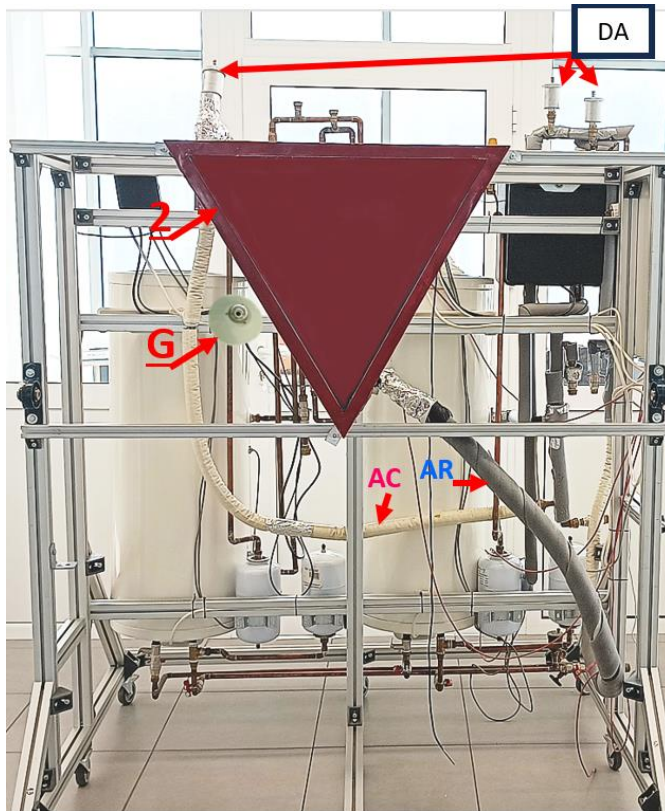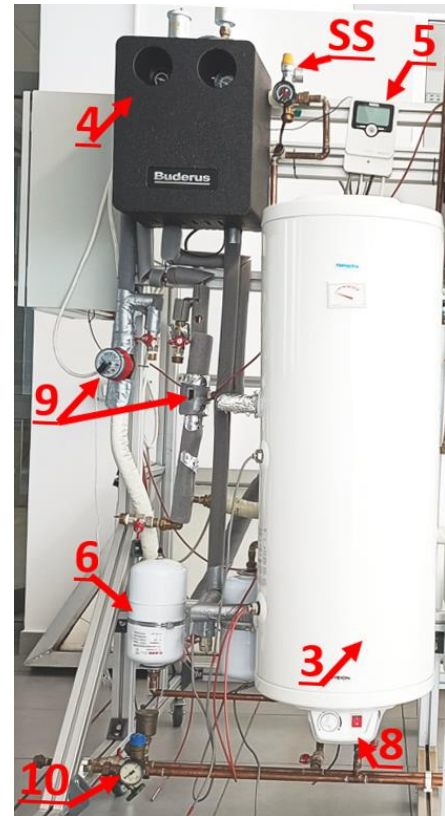| Designer	Denisa Rusea			Project title:	
Drawn	Denisa Rusea			SOLAR THERMAL SYSTEM FOR INDOOR TESTING	2023
Checked	Ion Vișa				
Approved	Ion Vișa		Data:24.01.2023		
UM mm.	UNIVERSITY "TRANSILVANIA" OF BRAȘOV			The title: FUNCTIONAL SCHEME	Revision 001

Fig.4.2. Scheme of the test stand

Fig. 4.3. Test stand and characteristic elements: a. Solar simulator; b. Positioning the stand in front of the vertical simulator; c. Front view of the test stand; d. View from behind the test stand.

Stages of testing

The simulator worked for about an hour to stabilize the test parameters (adjusting the flow rate, inlet and outlet temperature of the water in the solar thermal collector).

The 5 temperature steps used during the test and the potential inlet and outlet temperatures of the heat agent are established to obtain the desired differences. according to table 4.1. It is considered T_a of 30 °C because after the system stabilizes, the air around the collector gradually warms up. The temperature difference ΔT is the variable component against which the efficiency of the solar thermal collector results and has the relationship:

$$\Delta T=[(T_{in}+T_{out})/2]-T_a \qquad (4.4)$$

Table 4.1. Values given as an example for the 5 steps of temperature differences used during the laboratory test

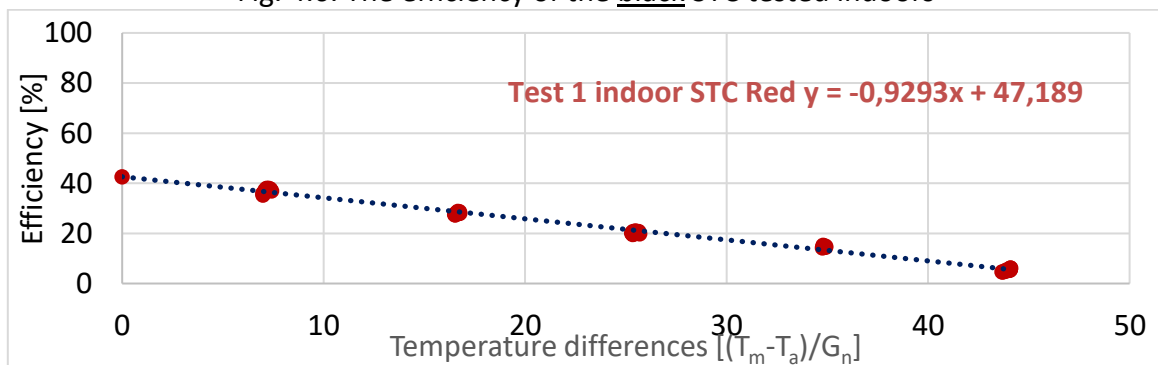| T_{in}	T_{out}	T_a	ΔT
[°C]	[°C]	[°C]	[°C]
30	30	30	0
40	40	30	10
50	50	30	20
60	60	30	30
70	70	30	40

To obtain these differences, the following steps are defined in collector testing:

1. For ΔT =0°C, when T_a =30°C, T_{in}= T_{out} , after half an hour the system stabilizes and the collector starts to heat the heating medium, so T_{out} >T_{in}; The system is allowed to run for another 15 min. until no large differences are observed in the temperature of the thermal agent at the outlet of the manifold, (during this time the moditorized data is read and the temperature values at the inlet/outlet of the manifold are noted). Thus, the system is allowed to stabilize for 10 min., and in the next 5 min. the monitored data is read.
2. The system is prepared for the next temperature step and the previous procedure is resumed.

Testing is done in turn, but in the same way for both black and red absorbent plate collectors.

The experimental data are monitored with a frequency of 1 min throughout the duration of the tests and represented graphically in Fig.4.4 for black STC and Fig. 4.5 for red STC.

To obtain the nominal efficiency of the STC, the monitored parameters are processed in order to represent them graphically in the form of a linear function (Fig. 4.6 and Fig. 4.7).

Fig.4.4. Variation of parameters in indoor testing of <u>black</u> STC

Fig.4.5. Variation of parameters in indoor testing of <u>red</u> STC

Fig. 4.6. The efficiency of the <u>black</u> STC tested indoors

Fig. 4.7. The efficiency of the <u>red</u> STC tested indoors
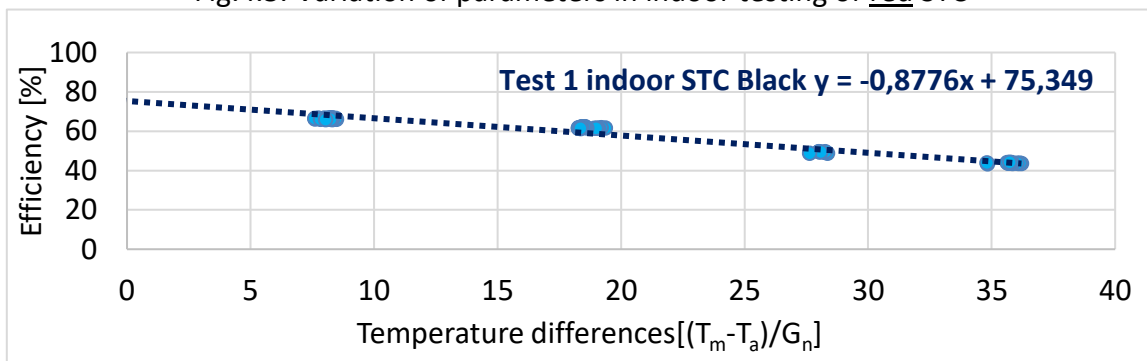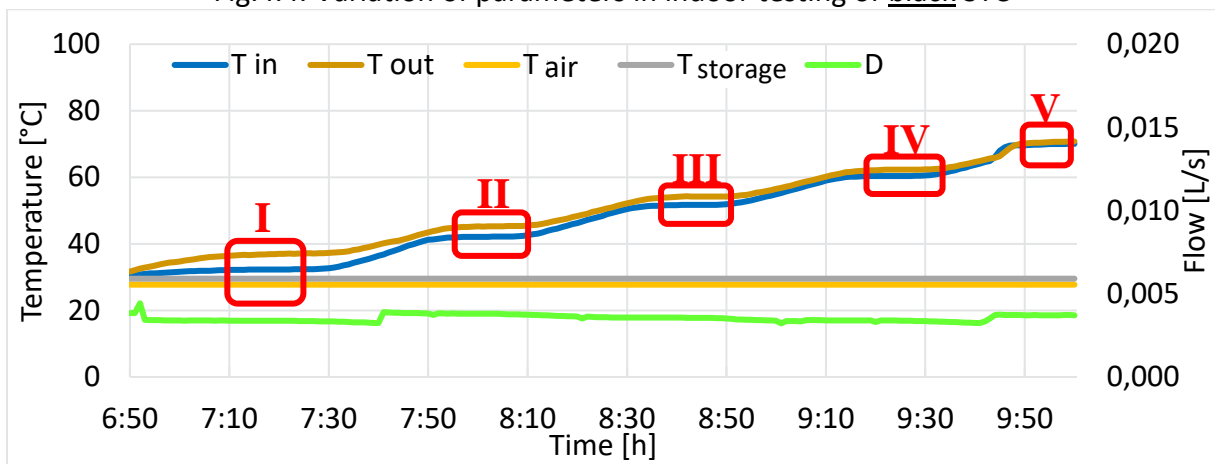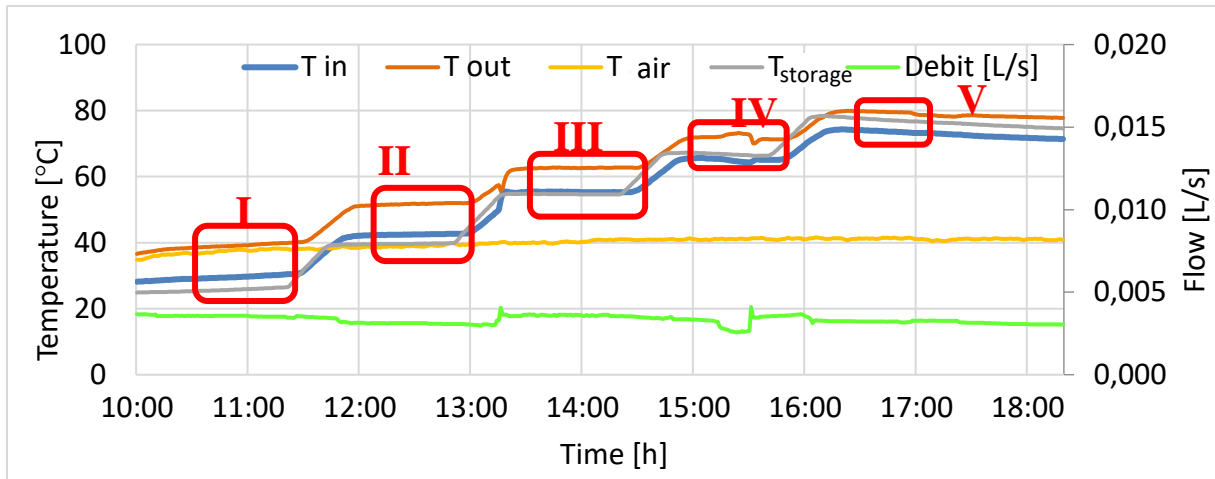
Comparison of the resulting indoor efficiency vs indoor numerical simulation

The simulated results are similar to the indoor testing results for both collectors where an error of: 3.02% was obtained for the <u>black</u> collector, for indoor testing an efficiency of 75.35% was obtained, and in the simulation the result was 73.14% (Fig .4.10).
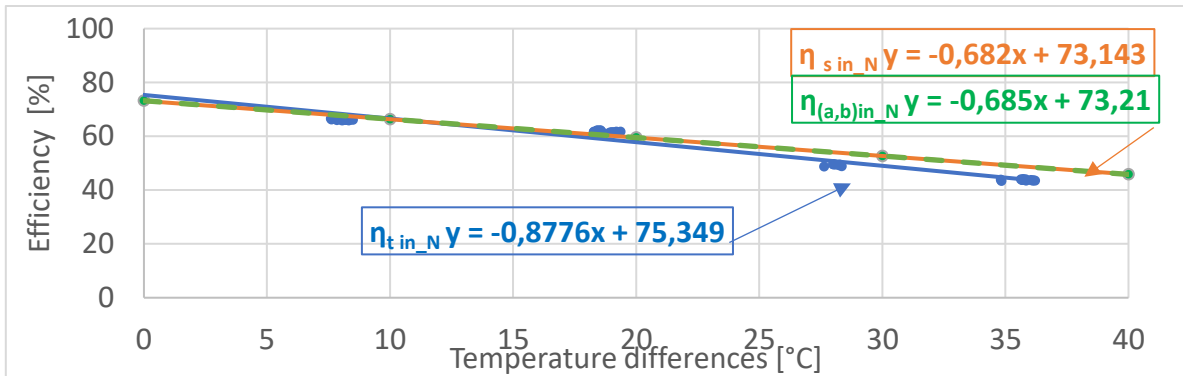

Fig. 4.8. Comparison of efficiency results obtained for indoor <u>black</u> STC - simulation

For the <u>red</u> triangular solar collector, an efficiency of 42.6% was obtained indoors, and 47.004% in the simulation, resulting in an error of 9.37% (Fig. 4.11).
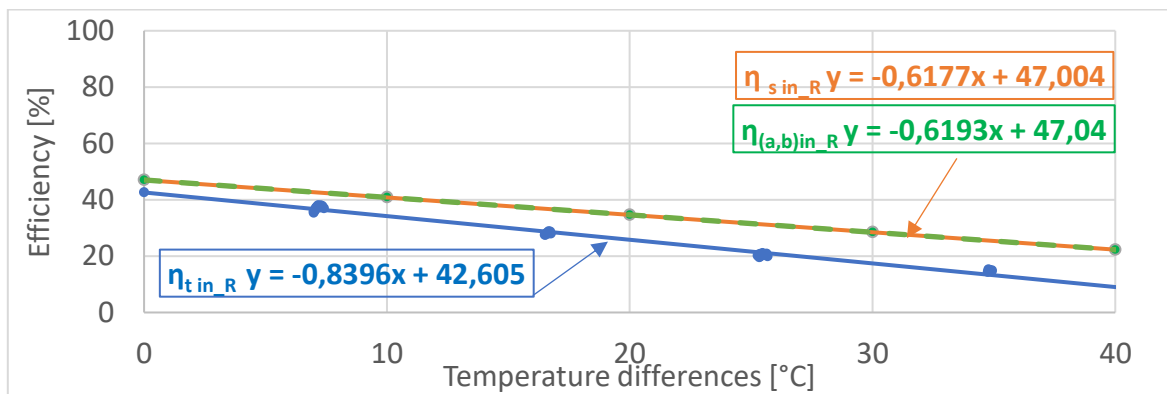
Fig. 4.9. Comparison of the efficiency results obtained for the indoor <u>red</u> STC - simulation

4.2. Outdoor testing

The outdoor experimental testing was carried out using the existing outdoor stand in the laboratory of the RESREC Research Center of Transilvania University in Brașov. The two flat flat solar thermal collectors with the black and red absorber were mounted on the southern facade of the stand building (Fig. 4.10).

The scheme of the test stand is shown in Fig. 4.11. and the elements detailed in Fig.4.12.

Fig. 4.10 Layout of the red and black STC on the southern facade of the
L7 RESREC laboratory annex

The components that make up the test stand can be classified into main, secondary and ancillary elements as in the case of the indoor stand:

a.   Main components:

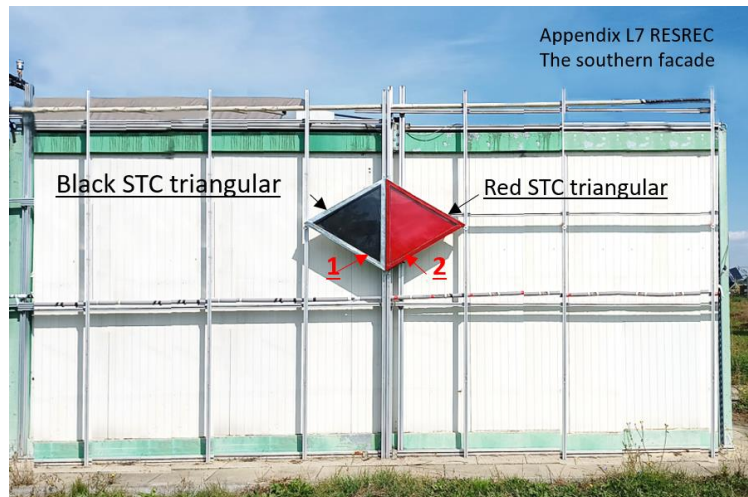1,2   The solar thermal collectors - with black absorber and red absorber arranged on the southern facade of the annex building having a common side, the Boiler/Storage - with the role of storing thermal energy, having an electrical resistance used as an additional heating source;

4.   Hydraulic pump - with the role of ensuring the circulation of the thermal agent through the solar collector during testing;

5.   Controller - which monitors the intensity of solar radiation;

6.   Expansion vessel - to take the increase in fluid volume after its heating and expansion;

b.   Secondary components:

7.   Electric resistance for heating the boiler;

8.   Flowmeter for black STC – for measuring and monitoring the flow of the heating agent;

9.   Flowmeter for red STC – for measuring and monitoring the flow of the heating agent;

10.   Manometer – for measuring hydraulic pressure in the system;

B   Pyrheliometer for monitoring the intensity of direct solar radiation;

Dh   Pyranometer with shade for monitoring the intensity of diffuse solar radiation in the horizontal plane;

T   Temperature sensors - which have the role of measuring the temperature of the heating agent. They are located at the inlet/outlet of the heat agent from the collector and from the boiler, and sensors located outside to monitor the air temperature;

c.   Auxiliary components:

DA	Automatic vent - used to release the air from the solar thermal collector circuit installation;
SS	Pressure valve - 10 bar - to release the pressure from the system in case it increases with the heating of the heating agent;
⋈	Valves for filling/evatuating the installation;
〰	Rigid copper pipe connections – through which the heat agent flows, properly insulated to minimize heat loss through the pipes.

The test procedure includes:

Step 1. **Carrying out pressure tests in the circuit.**
Step 2. **Checking the temperature sensors.**
Step 3. **Connecting the collector system to the hydraulic system.**
Step 4. **Adjusting the flow rate.**
Step 5. **System stabilization (approx. 1 week).**
Step 6. **Monitoring test parameters.**
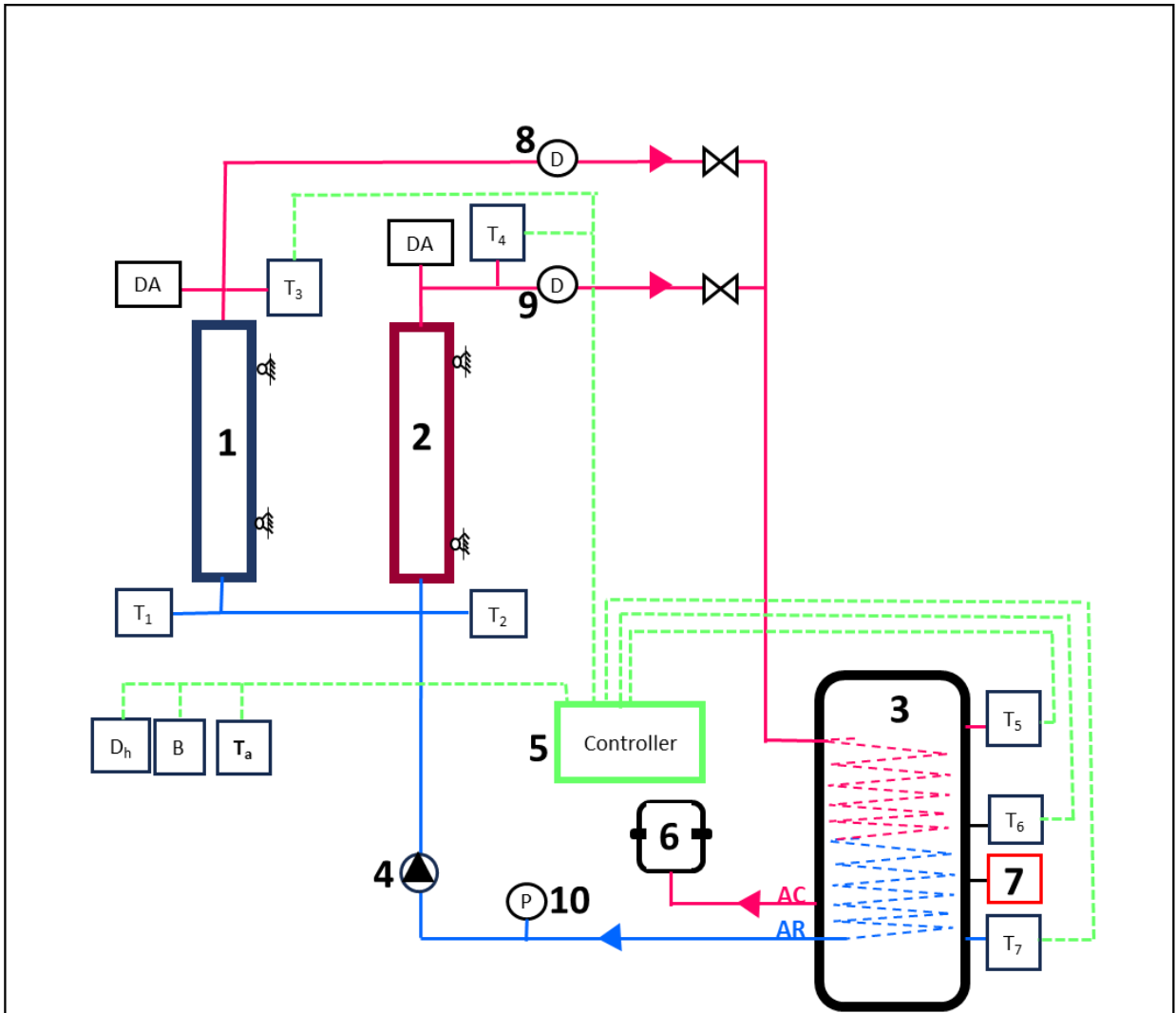
Monitored parameters:

- the inlet/outlet temperature of the heating agent from the STC: T_{in}, T_{out};
- temperature of the thermal agent in the boiler, T_b;
- the air temperature in the outdoor environment, T_a;
- intensity of direct (B) and diffuse solar radiation in the horizontal plane (D_h);
- flow rate of the heating agent, $\dot{m}$;
- pressure in the solar circuit, p.

Stages of testing

Outdoor testing depends on weather conditions on the day. In order to obtain the maximum efficiency of the STC, it is necessary that the testing takes place during a period of days with clear skies, when the collector can receive direct radiation from the sun. So, compared to indoor testing, outdoor testing takes place over a longer period of time.

In order to obtain the same temperature differences used in indoor testing, the following steps are defined in collector testing:

1. For $\Delta T = 0°C$, when $T_a \approx 20°C$, $T_{in} = T_{out}$, the system is allowed to operate for a week during which the weather is monitored, as one or more clear days are required for a valid test.
2. 2. The system is prepared for the second temperature step, for $\Delta T = 10°C$. If it holds $T_a \approx 20°C$, then the temperature of the fluid at the inlet of the manifold must increase by 10°C. The electrical resistance of the boiler is switched on and the heat agent in the boiler is heated with 10 °C. When the temperature in the boiler has reached the desired value, the resistance and the thermostat stop. The system is again allowed to stabilize. The period of stabilization and heating of the thermal agent by the collector also depends on the weather conditions, several clear days being necessary. After obtaining the results, proceed to the 3rd stage.
3. The procedure is repeated until the tests are performed for all temperature steps.
4. The data of the monitored parameters are then used to obtain the efficiency values of the solar thermal collector.

SUMMARY

B	Pyrheliometer
D_h	Pyranometer with shade
DA	Automatic vent
T	Temperature sensor for monitoring
⋈	Water tap
	Safety valve
AR	Cold water supply circuit
AC	Hot water supply circuit
—— (blue)	Inlet circuit pipe
—— (pink)	Outlet circuit pipe
- - - (green)	Monitoring circuit

Pos.	Name	Obs.
10	Manometer	
9	Flowmeter for red STC	
8	Flowmeter for black STC	
7	Electric resistance for heating	
6	Expansion tank	
5	Controller for the solar circuit	
4	Hydraulic pump	
3	Tank/ storage	
2	Red triangular thermal solar collector	
1	Black triangular thermal solar collector	

Designer	Denisa Rusea			Project title:	2023
Drawn	Denisa Rusea			SOLAR THERMAL SYSTEM FOR OUTDOOR TESTING	
Checked	Ion Vișa				
Approved	Ion Vișa		Data:24.01.2023		
UM mm.	UNIVERSITY "TRANSILVANIA" OF BRAȘOV			The title: FUNCTIONAL SCHEME	Revision 001

Fig.4.11. Scheme of the outdoor test stand

a.
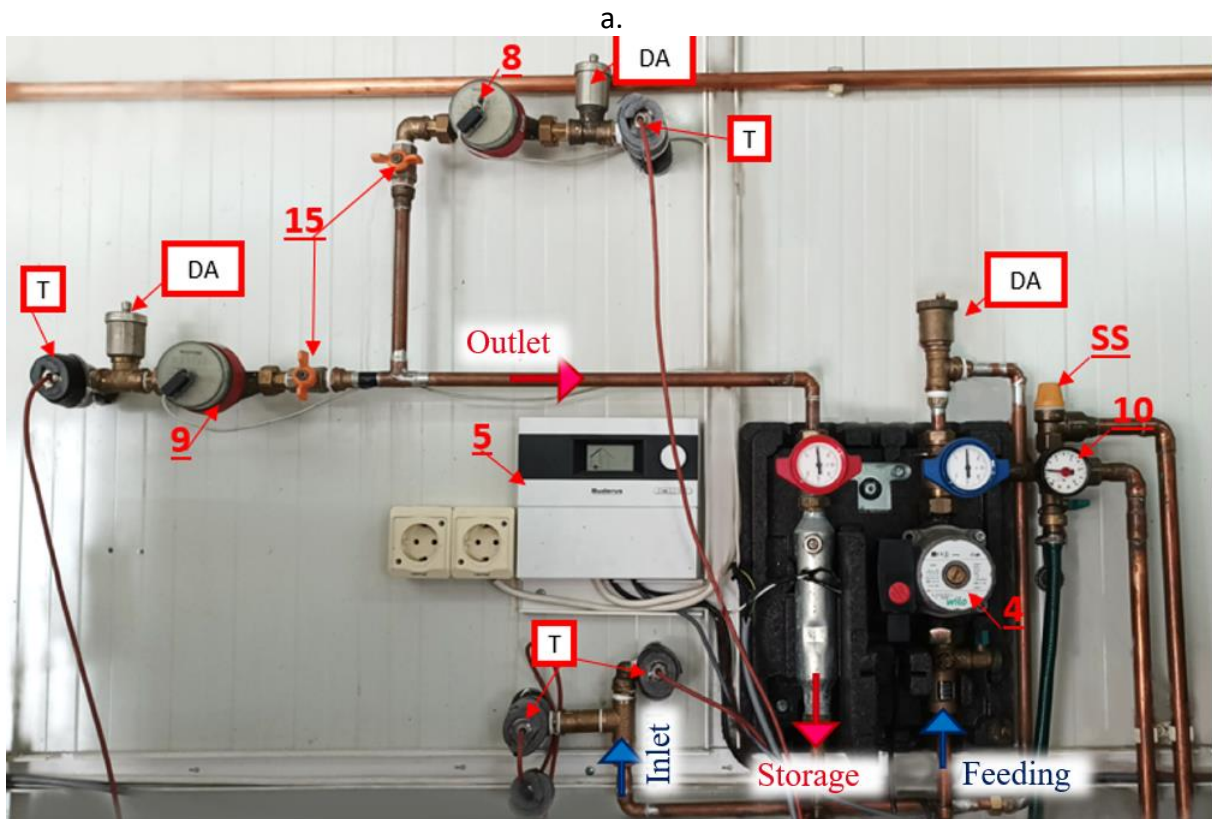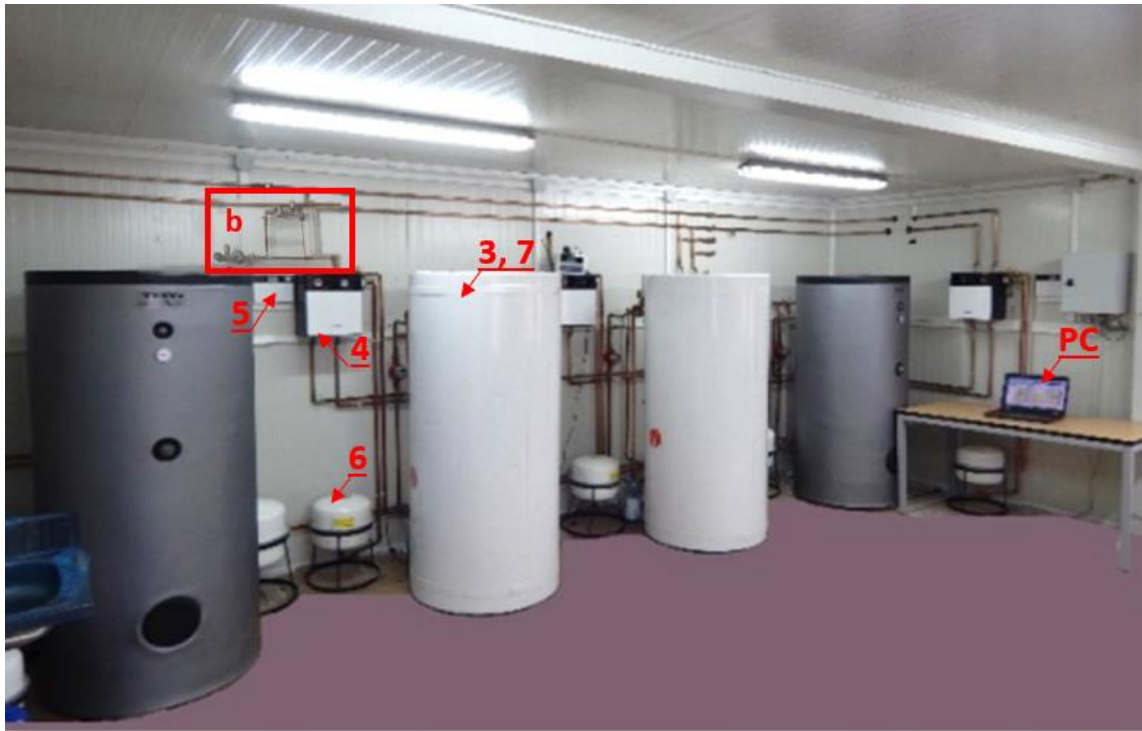
b.

Fig. 4.12. Details of the test stand and the component elements: a. Location of the test stand inside the L7 Laboratory; b. Test stand circuit and components.

To calculate the efficiency of solar thermal collectors in the vertical plane, it is necessary to calculate the global solar radiation intensity in the same plane (in Fig. 4.13) with the help of which the input solar power is calculated, and with the help of the monitored parameters of the thermal agent, the thermal power of exit.

Thus, for the triangular thermal solar collector with black absorber, a nominal efficiency of 65.5% is obtained after outdoor testing, the variation can be observed graphically in figure 4.14. The same procedure was used to obtain the efficiency of the solar thermal collector with red absorber, resulting in a nominal efficiency of 45.25% (Figure 4.15).
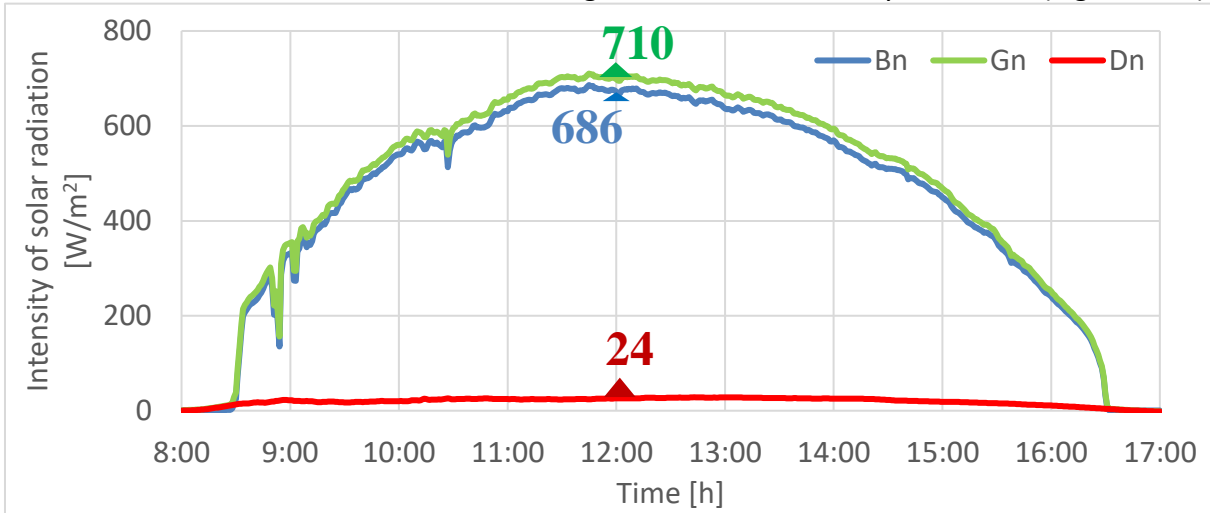

Fig.4.13 The intensity of direct, diffuse and global solar radiation in the vertical plane
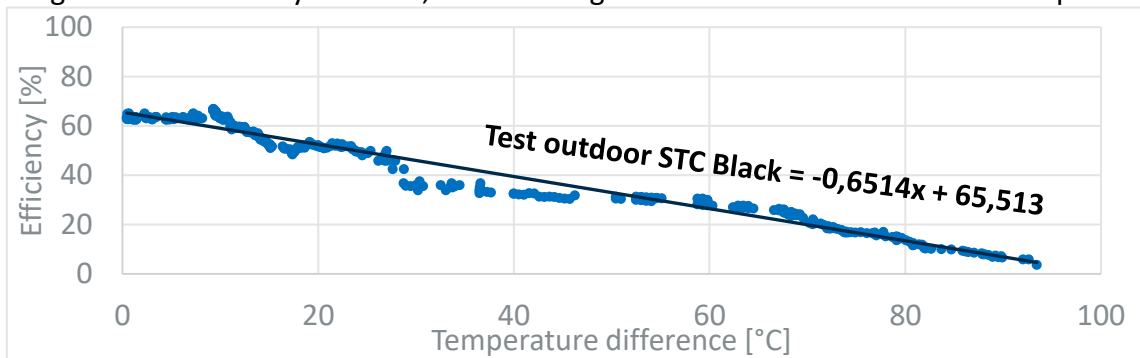

Fig. 4.14. Efficiency of the black triangular thermal solar collector after outdoor testing
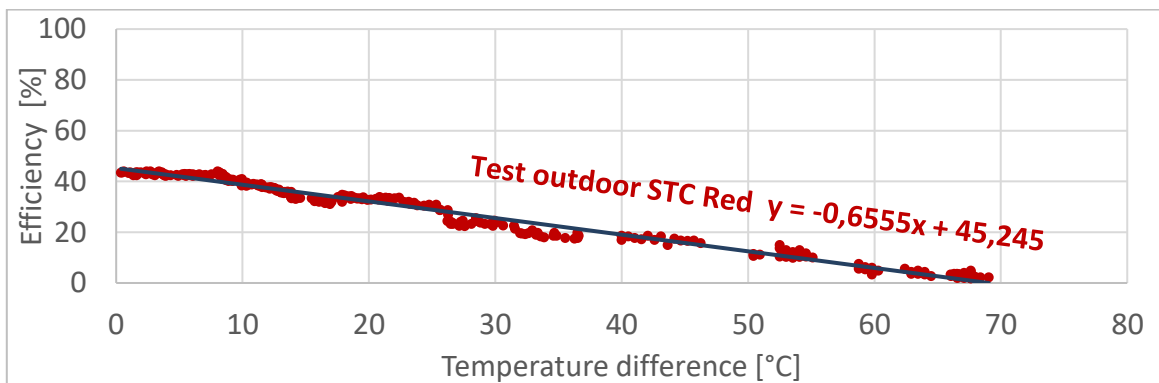

Fig. 4.15. The efficiency of the red triangular thermal solar collector after outdoor testing

Comparison of the resulting outdoor efficiency vs outdoor numerical simulation

Comparing the outdoor experimental results and the numerical calculations performed to simulate the outdoor testing, a difference given by the relative error resulted; the difference is due to different environmental conditions, varying solar radiation intensity and different absorbance for the two colors of the absorbent plate.

The results are obtained according to Fig. 16 and Fig. 17.: the maximum (nominal) efficiency of the solar thermal collector with black absorber is **65.5%,** and for the one with red absorber is **45.25%,** representing a relative error of **9.9%** for the collector with black absorber and **3.75%** for the collector with red absorber.
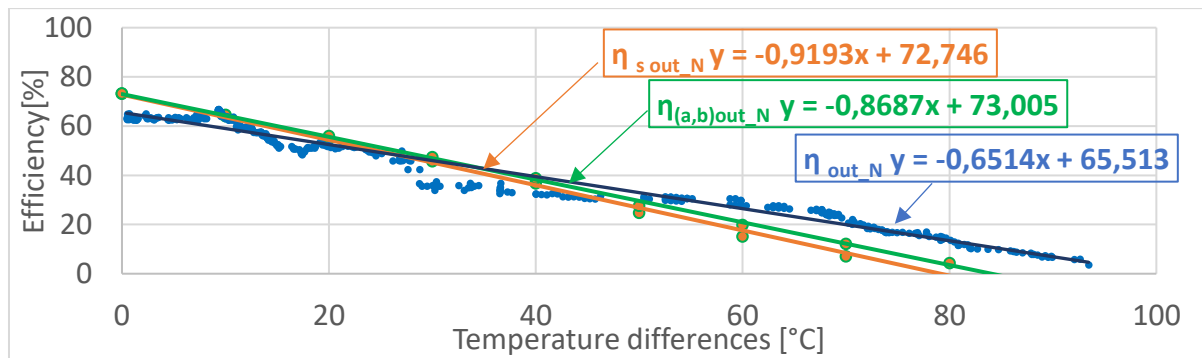
Fig. 4.16. Comparison of the efficiency results obtained for STC <u>black</u> outdoor - simulation
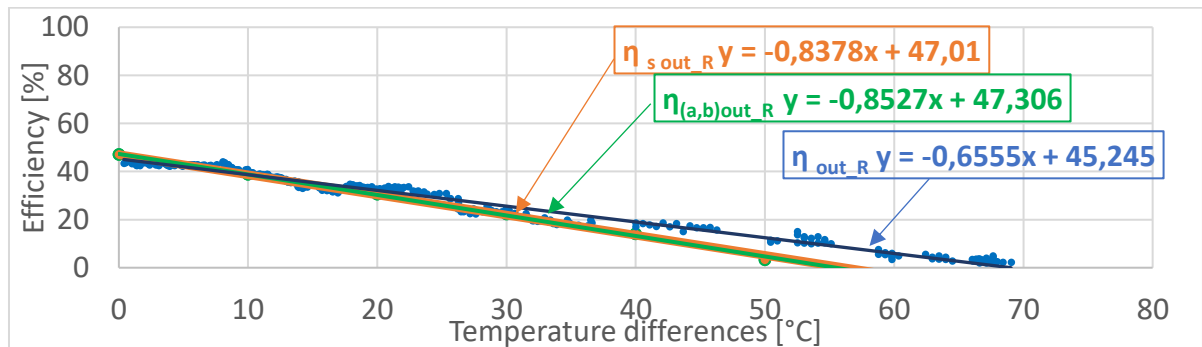
Fig. 4.17. Comparison of the efficiency results obtained for STC <u>red</u> outdoor - simulation

Comparison of indoor vs outdoor results vs numerical simulations

The experimental results are compared with the numerical simulations according to the Duffie&Backman model, but also according to the η(a,b) formula. Graphical interpretation is available in Fig. 4.18 for the black collector and Fig. 4.19 for the red collector.

For both tests, the simulations performed have higher values than the actual results because the actual test conditions are different than the model considered ideal in the simulation. Numerical simulations can be adjusted using absorption coefficients resulting from comparing experimental vs simulation results, in order to obtain numerical simulations closer to the real model.

Thus, the mathematical model can be adjusted in order to obtain the efficiency of flat solar thermal collectors of different colors, the simulations depending a lot on the absorption coefficient of each individual color.
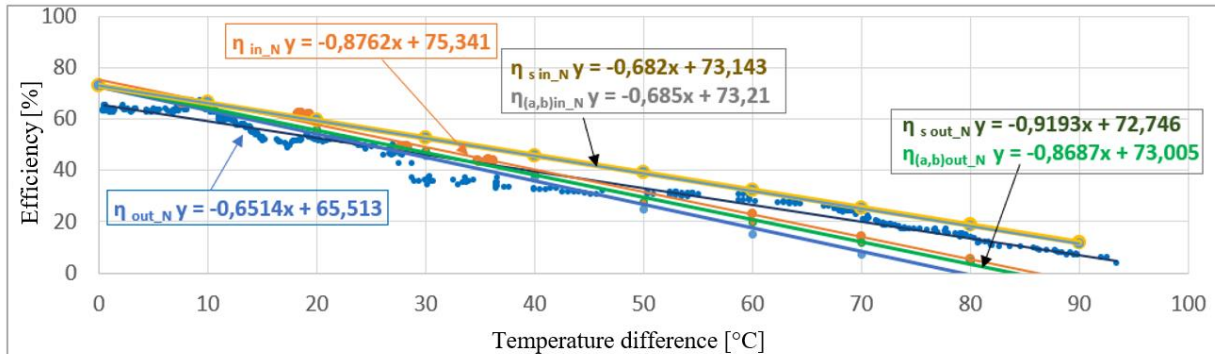
Fig. 4.18. Comparison of efficiency results in/outdoor vs simulations for <u>black</u> STC
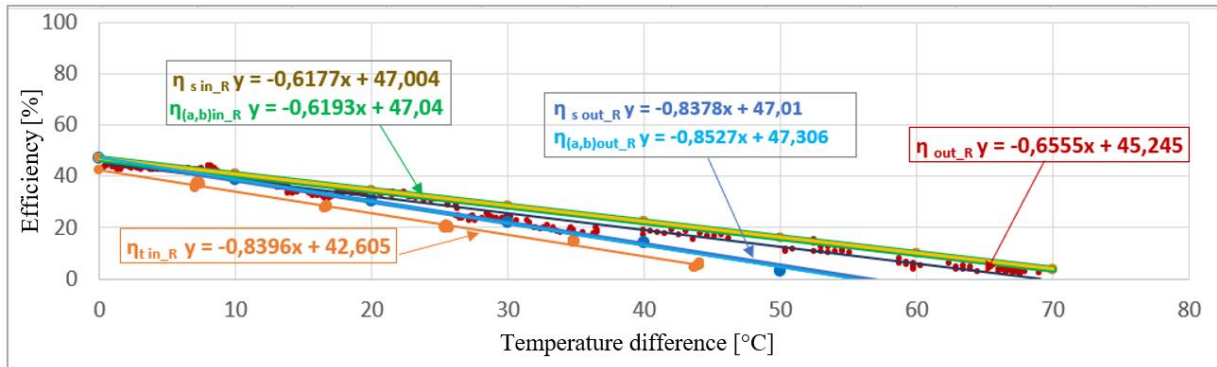
Fig. 4.19. Comparison of efficiency results in/outdoor vs simulations for <u>red</u> STC

The coefficients ,,a" and ,,b" from the formula of the adapted mathematical simulation, are taken from the linear equation resulting from the graphic representation of the outdoor efficiency in the form of the first-degree function. Thus, from the nominal efficiency results:

η_{in_N} y = -0.8776x + 75.35   =>   a=75.35/100 =0.753
$\eta_{t\,in\_R}$ y = -0.8396x + 42.605   =>   a= 42.605/100 =0.426
η_{out_N} y = -0.6514x + 65.513   =>   a= 65.513/100 =0.655
η_{out_R} y = -0.6555x + 45.245   =>   a= 45.25/100 =0.452

Knowing $a=\alpha\tau F_R$, by dividing the coefficient ,,a" to (τF_R) the two absorption coefficients result:
- in the indoor case, for the black collector, the constant,,a" from outdoor testing is 0.753, which results in an absorption coefficient of 0.98in the case of the red collector, the constant,,a" from outdoor testing is 0.426, which results in an absorption coefficient of 0.54.
- in the outdoor case, for the black collector, the constant ,,a" from outdoor testing is 0.655, resulting in an absorption coefficient of 0.85; in the case of the

red collector, the constant „a" from the outdoor testing is 0.452, which results in an absorption coefficient of 0.57.

Therefore, from the outdoor testing, the absorbance of the collectors is 85% for black, respectively 57% for red, and from the indoor testing, it emerges: 97% for black, respectively 54% for red. Remembering that the numerical simulations were performed for 95% black absorption and 60% red absorption, the errors can be adjusted by updating the calculations for the absorbance values resulting from comparing the tests with the simulations.

The summary of results is available in table 4.2. The relative error of the Duffie&Backman numerical simulation vs testing is calculated, respectively the calculation error between the two simulations.

Table 4.2. Summary of test results vs numerical simulations

Indoor testing vs simulations			
STC_Black		**STC_Red**	
η t in_N	75.35	η t in_R	42.6
η s in_N	73.14	η s in_R	47.004
η (a,b) in_N	73.21	η (a,b) in_R	47.04
RE(η t in_N vs η s in_N)[%]	3.02	**RE(η t in_R vs η s in_R)[%]**	9.37
RE(η s in_N vs η (a,b) in_N)[%]	0.09	**RE(η s in_R vs η (a,b) in_R)[%]**	0.08
Outdoor testing vs simulations			
STC_Black		**STC_Red**	
η t out_N	65.51	η t out_R	45.25
η s out_N	72.75	η s out_R	47.01
η (a,b) out_N	73.005	η (a,b) out_R	47.306
RE(η t out_N vs η s out_N)[%]	9.94	**RE(η t out_R vs η s out_R)[%]**	3.75
RE(η s out_N vs η (a,b) out_N)[%]	0.36	**RE(η s out_R vs η(a,b) out_R)[%]**	0.63

For both tests, the simulations performed have higher values than the actual results because the actual test conditions are different than the model considered ideal in the simulation. Numerical simulations can be adjusted using absorption coefficients resulting from comparing experimental vs simulation results, in order to obtain numerical simulations closer to the real model.

Thus, the mathematical model can be adjusted in order to obtain the efficiency of flat solar thermal collectors of different colors, the simulations depending a lot on the absorption coefficient of each individual color.

5. Final conclusions. Original contributions. Dissemination of results. Future directions.

The main conclusions of the conducted research, original contributions made through this thesis, the dissemination of the obtained results and possible future directions are presented in the following paragraphs.

6.1. Final conclusions

The main conclusions for the development and implementation of collectors of various shapes and colors in the built environment to ensure the need for thermal energy and increase architectural acceptance are the following:

a. The increase in the amount of thermal energy produced by systems located on buildings (facades and roofs) requires the use of unconventional solar thermal collectors of different shapes and colors.

b. Triangular and trapezoidal STC represent a feasible solution in this context.

c. At the same time, different colors can be used to asure the architectural acceptance.

d. Triangle and trapezoid STC systems allow their use in a wide variety of buildings (residential buildings, apartment blocks, administrative buildings, heritage buildings), facade and roof configurations.

e. The identified structures can be applied as stylized representations of various artistic images or as a simulated 3D effect on building facades which increases architectural acceptance.

f. The main parameters and optimal dimensions of the equilateral triangular STC for a certain size type resulted from the study of thermal losses and the factors that influence them.

g. The magnitude of the total heat losses, the heat extraction factor and the transmittance-absorbance product of the color absorbance and glass led to a simple formula for calculating the efficiency of the triangular serpentine of STC. The formula can be developed for various types, sizes and colors of triangular STC.

h. The error between the STC efficiency calculated with the two methods (Duffie&Backman vs. the proposed formula) is insignificant, under 1%.

i. The theoretical results were validated by the indoor and outdoor experimental testing of the black and red triangular STC by adapting the existing stands in the RESREC Research Center.

j. The calculated and experimentally determined nominal efficiencies fall within the following limits: **for black STC the calculated efficiency is 73 %, and for red STC the efficiency is 47%.**

k. Indoor testing at constant intensity of soalr radiation of 950 W/m^2 resulted in the nominal efficiency of **75.34% for black STC and of 42.6 % for red STC,** so values significantly equal to those obtained by calculation.

l. Outdoor testing in real and clear sky conditions at the average radiation of the median interval of the considered days (an average radiation of 750 W/m^2) resulted in the nominal efficiency of **65.5% for the black STC and 45.25% for the red STC**. The larger differences between the calculated efficiencies and those obtained outdoors are explained by the different weather conditions compared to indoor testing.

m. Thus, the results obtained by calculation were validated by indoor and outdoor testing with relative errors below 10%.

n. The optimally designed and experimentally tested triangular STC can be passed for the prototype phase with a view to technological transfer to the economic environment.

6.2. Original contributions

The original contributions made by this thesis on increasing the amount of thermal energy and architectural acceptance through the development and use of solar thermal collectors of unconventional shapes and different colors are as follows:

a. Detailed analysis of thermal energy production systems in the built environment.

b. Design, development and optimization of the equilateral triangular collector with internal coil.

c. Identification of all subassemblies consisting of two or three STCs.

d. Using subassemblies to obtain complex shapes of stylized images or simulating 3D effect in the built environment for building facades and roofs.

e. Numerical calculation of the influence of the constructive parameters of the triangular collector.

f. Simplifying the nominal efficiency calculation relationship.

g. Dimensional design and construction of optimal triangular solar collector with serpentine.

h. Indoor and outdoor testing by adapting the existing stands.

i. Validation of the models of equilateral triangular solar thermal collectors proposed in this thesis.

6.3. Dissemination of results

The results of the conducted research were highlithed as follows:

a. Publication of 3 scientific papers:

1. Rusea, I., Moldovan, M., Vișa , I., ,,*Novel Pseudo 3D Design of Solar Thermal Facades with Triangle and Trapeze Solar Thermal Collectors for Increased Architectural Acceptance*", Springer - Mechanisms and Machine Science , vol.134, p.27-36, Proceedings of I4SDG Workshop2023 IFToMM for Sustainable Development Goals 2023.

2. Moldovan, M., Rusea, I., Vișa, I., ,,*Optimising the thickness of the water layer in a triangle solar thermal collector*, Renewable Energy, Vol. 173, pp 381-388, 2021 (IF 8.7).

3. Moldovan, M., Vișa, I., Rusea, I. D., *The influence of the Solar Thermal Collectors integrated into the building facade on the building thermal energy demand across Europe* ", Journal of Science and Art, Vol. 1, No. 50, pp 203-214, 2020.

4. Rusea, I. D., Moldovan, M., Vișa, I.,,,*Test and Simulation of efficiency of triangle solar thermal collectors with internal serpentine* ", 7th edition of the Conference for Sustainable Energy, CSE 2023, in Brașov. (proposed for publication at Renewable Energy journal)

b. Participation in national and international conferences:
1. Conference for Sustainable Energy, Brașov, CSE 2023.

6.4. Future directions

The results obtained through the conducted scientific research open new directions in the field of conception, development and implementation of equilateral triangular solar thermal collectors with internal serpentine and the assemblies formed by them with similar trapezoidal collectors.There are as follow:

a. Development and testing of multi-color absorption collectors.

b. The use of STC absorbance and transmittance obtained by experimental determination in the calculation of the nominal efficiency of STC and their indoor and outdoor testing.

c. The development of new type-dimensions of equilateral triangular collectors with serpentine and their study through calculation and indoor/outdoor experimental research, for the generalization of the nominal efficiency calculation method proposed in the paper.

d. Development of new types of non-conventional STCs (e.g. triangular/rectangular trapezoidal) to ensure a higher degree of reproduction of the various models.

e. The development and study of assemblies of two triangle-trapezoid type collectors and their optimization for the development of prototype products transferable to the economic environment.

Bibliography (Selection)

17. Duffie J., Backman W., *„Solar Engineering of Thermal Proces Ediția a IV-a",* Wisconsin-Madison: Wiley, 2006

27. Hill Jamie.E., Kusuda T., *„Method of testing for rating solar collectors based on thermal performance",* Washington, D.C: Center of building technology national Bureau of standards, 1974

28. Isac Luminita, Panait Ramona , Enesca Alexandru , Bogatu Cristina , Perniu Dana , Duta Anca, *„Development of Black and Red Absorber Coatings for Solar Thermal Collectors",* Conference on Sustainable Energy, 2017

31. Kalogirou S., Tripanagnostopoulos Y., Souliotis M., *„Modeling and Simulation of Solar Systems Employing Collectors with Colored Absorber."* Research Gate, 2017

32. Kalogirou A.S., *„Solar Energy Engineering"* ,Processes and Systems, Academic Press,Elsevier, USA, 2009

33. Kalogirou S., Tripanagnostopoulos Y., Souliotis M., *„Performance of solar systems employing collectors with colored absorber,"* Energy and Buildings, vol. 37., p.824-835, 2005

41. Moldovan Macedon, Vișa Ion, **Rusea Ioana Denisa,** *„The influence of theSolar Thermal Collectors integrated into the building facade on the building thermal energy demand across Europe",* Journal of Science and Art, Josa, 2020

42. Moldovan, M., **Rusea**, I., Vișa , I., *„Optimising the thickness of the water layer in a triangle solar thermal collector",* Renewable Energy, Vol. 173, pp 381-388, 2021

49. Probst Munari Maria Cristina, Roecker Christian, *„From Thermal Collectors Integration to Active Façade Systems."* , PLEA2007 - The 24th Conference on Passive and Low Energy Architecture. Singapore, 2007

53. **Rusea**, I., Moldovan, M., Vișa , I., *Novel Pseudo 3D Design of Solar Thermal Facades with Triangle and Trapeze Solar Thermal Collectors for Increased Architectural Acceptance,* 2023

64. Vișa et al. , *„System of modular polygonal planar solar panels for integration into facades"* , Patent proposal no. A/00156 / 18.02.2013

65. Vișa Ion, Comsit Mihai, Duta Anca, *„Urban acceptance of facade integrated novel solar thermal collectors",* Energy Procedia 48 p.1429 – 1435, 2014

66. Vișa Ion, Duta Anca, Comsit Mihai, Moldovan Macedon, Ciobanu Daniela, Saulescu Radu, Burduhos Bogdan, *„Design and experimental optimisation of a novel flat plate solar thermal collector with trapezoidal shape for facades integration",* Applied Thermal Engineering, 2015

67. Vișa I., Jaliu C., Duță A., Neagoe M., Comșiț M., Moldovan M., Ciobanu D., Burduhos B., Săulescu R. Brașov. *„The Role of Mechanisms in Sustainable Energy Systems",* Editura Universității Transilvania din Brașov, Brașov,2015

68. Vișa, Ion, Anca Duta. *"Innovative Solutions for Solar Thermal Systems Implemented in Buildings."* Energy Procedia, Volume 85, January 2016.

69. Vișa Ion, Moldovan Macedon, Comsit Mihai, Neagoe Mircea, Duta Anca, *„Facades integrated solar-thermal collectors – challenges and solutions",* Energy Procedia 112 p.176 – 185, 2017

70. Vișa, Ion, Anca Duta. *"Nearly Zero Energy Communities."* Proceedings of the Conference for Sustainable Energy (CSE), Springer, 2017.